Geoscience Frontiers 17 (2026) 102256

Contents lists available at ScienceDirect

Geoscience Frontiers

journal homepage: www.elsevier.com/locate/gsf

Research Paper

Rainwater accumulation model related to tectono-stratigraphic assessment for bradyseism at Campi Flegrei, Italy

Nicola Scafetta [a,*], Annamaria Lima [a], Alfonsa Milia [b], Frank Spera [c], Robert J. Bodnar [d], Benedetto De Vivo [a,d,e,f], Linda Daniele [g]

[a] Dipartimento di Scienze della Terra, dell'Ambiente e delle Risorse (DiSTAR), University of Naples Federico II, Complesso Universitario di Monte Sant'Angelo, Via Cintia 26, 80126 Naples, Italy
[b] Istituto di Scienze Marine, ISMAR-CNR, Calata Porta di Massa, Porto di Napoli 80133, Italy
[c] Department of Earth Science and Earth Research Institute, University of California, Santa Barbara, CA 93106, USA
[d] Department of Geosciences, Virginia Tech, 4044 Derring Hall, Blacksburg, VA 24061, USA
[e] Nanjing University, Nanjing 210023, China
[f] Hubei Polytechnic University, Huangshi 435003, China
[g] Department of Geology, FCFM, University of Chile, Santiago, Chile

ARTICLE INFO

Article history:
Received 15 September 2025
Revised 24 December 2025
Accepted 13 January 2026
Available online 17 January 2026

Keywords:
Pozzuoli-Solfatara bradyseism
Anticline stratigraphic structure
Hydrological model
Meteoric water infiltration
Pyroclastics

ABSTRACT

The Campi Flegrei (CF) volcanic system near Naples, Italy, poses a significant hazard due to bradyseism — a slow vertical ground deformation resulting in either uplift or subsidence. Indeed, between January 2005 and January 2025, the urban area of Pozzuoli experienced approximately 1.4 m of uplift (GNSS RITE Station). The bradyseism is driven by a combination of hydrothermal and magmatic processes, whereby pressurized magmatic fluids generated by deep magma crystallization accumulate beneath an impermeable layer that regulates fluid exchange between upper hydrostatic and lower lithostatic systems. This study introduces a new perspective through a detailed reconstruction of the stratigraphic-tectonic architecture of the CF area that enables identification of structural controls on seismicity, deformation, and fluid migration, and the role of meteoric water. Seismicity beneath the Pozzuoli-Solfatara area occurs at shallower depths near the top of an anticline, whereas deeper earthquakes in Pozzuoli Bay occur in synclinal environments. The anticline beneath Pozzuoli facilitates hydrothermal fluid pressurization in two main reservoirs beneath two relatively impermeable units. The shallow reservoir, referred to as Unit C, is located at a depth of approximately 1.0 to 2.0 km and acts as a reservoir for meteoric water infiltration. The deeper reservoir, referred to as Unit A, occurs at a depth of about 2.0 and 4.0–4.5 km, where magmatic fluids generated by second boiling in the underlying magma accumulate. An impermeable unit of marine sediments, referred to as Unit B, is located at ~ 2 km depth and separates Units A and C. The shallow reservoir is bounded at the top by a relatively impermeable unit mainly made up of pyroclastic deposits. We developed a simplified hydrogeological model using rainfall data dating back to 1950 to assess the role of meteoric water in bradyseism at CF. We found a strong correlation between subsurface water infiltration and vertical ground deformation observed at the Pozzuoli RITE Station, which corresponds to the crest of the anticline. Our results suggest that meteoric water contributes to interannual uplift fluctuations of up to ~ 5 cm and accounts for over 20% of the total uplift recorded between 2005 and 2025. Furthermore, a shortening of recharge time-lag — from about four years to three years since 2010 — indicates enhanced fracturing and infiltration rates. These findings highlight the previously underestimated role of meteoric water in driving deformation and seismicity at CF. Our results also suggest that geoengineering involving targeted surface drainage interventions could mitigate ongoing ground instability and seismic hazards in the region.

* Corresponding author.
E-mail address: nicola.scafetta@unina.it (N. Scafetta).

https://doi.org/10.1016/j.gsf.2026.102256

1. Introduction

The Campanian active volcanic region, encompassing the Campi Flegrei (CF) and the Somma-Vesuvius complexes in the province of Naples (Italy), represents an area of considerable risk, as over three million people are exposed to significant volcanic and seismic hazards (De Vivo and Rolandi, 2020; Carlino, 2021). Currently, CF is a major focus of concern due to accelerating ground uplift since 2005. CF is under constant monitoring and extensive study and has been the subject of numerous scientific investigations addressing its geochemical, geodetic, geological, seismological, and structural characteristics. While there is no consensus regarding the causes of this phenomenon, it is widely recognized that fluids within the geothermal system — of magmatic, marine, and/or meteoric origin — play a critical role (e.g., Caprarelli et al., 1997; Bodnar et al., 2007; Calìro et al., 2025).

Within CF, the Pozzuoli-Solfatara area has experienced the maximum uplift and most intense seismic activity. This shallow seismicity could have a hydrological influence associated with a decrease in the effective stress due to an increase in pore pressure that accompanies groundwater recharge (Casertano et al., 1976; Bonafede and Mazzanti, 1997; Wang and Manga, 2021). Shallow earthquake swarms at CF often exhibit relatively high b values in the Gutenberg-Richter scaling relation $\log_{10} N = a - bM$, where N is the cumulative number of earthquakes greater than magnitude M, and a and b are constants (Tramelli et al, 2024). High b values have been associated with pore pressure, thermal gradients and matrix heterogeneity (Warren and Latham, 1970; Wyss, 1973; Wiemer and McNutt, 1997). All of these factors may be significant at CF. Several studies have attributed seasonal variations of seismicity in other volcanic areas to groundwater recharge (e.g., Saar and Manga, 2003; Montgomery-Brown et al., 2019) via poroelastic effects. A correlation between precipitation and earthquakes (e.g., Roth et al., 1992; Jimenez and Garcia-Fernandez, 2000; Hainzl et al., 2006; Kraft et al., 2006; Husen et al., 2007) supports the idea that pore pressure changes caused by recharge processes can influence seismicity. For example, at the edge of Long Valley caldera, in California, large seasonal variations in precipitation occur, and seismicity rate is ~ 37 times greater during spring snowmelt than during the driest period of the year (Montgomery-Brown et al., 2019). At regional scales, changes in hydrological loading rate and induced pore pressure changes may contribute to seasonal variations in seismicity (Ueda and Kato, 2019). Underground water accumulation increases pore pressure, and can reduce the stability of existing faults, leading to both ground uplift and earthquakes mostly in geothermal regions where heated fluids expand, amplifying pressure, and contribute to ground uplift (Todesco, 2021). These phenomena are governed by the interplay of hydrogeological, mechanical, and geophysical factors (Wang and Manga, 2021).

Relative to the surrounding regions, CF experiences higher precipitation rates, which also leads to some exceptional flash floods (Fortelli et al., 2019). Morphologically, the CF region is characterized by numerous volcanic vents, such as the Astroni, upstream of the Solfatara area, that, as first hypothesized by Scafetta and Mazzarella (2021), could act as a funnel collecting large volumes of rainwater that can readily infiltrate the subsurface of the CF hydrothermal system through extensive fracturing in the upper 3 km (Cipriani et al., 2008), likely contributing to the surface uplift.

Although rainfall, atmospheric pressure variations and tidal oceanic loading have been posited as factors influencing seismic and volcanic activity (Mazzarella and Palumbo, 1989; Mastin, 1993; Farquharson and Amelung, 2020), these aspects have received relatively little attention at CF. Nevertheless, some studies have linked rainfall and tidal patterns to local seismicity recorded during the moderate uplift phases of bradyseism unrest between 2008 and 2020 (Petrosino et al., 2018; Scafetta and Mazzarella, 2021). Earlier epochs of uplift and increased concurrent seismic activity in 1970 and 1982 were preceded by anomalously large increases in oceanic loading and rainfall, although Palumbo (1985) could not clearly separate the rainfall and oceanic loading effects. The observation that periods of active uplift correlate with small changes in stress due to solar-lunar tidal effects (oceanic loading) and rainfall going back over a half-century indicates that the state of stress at depth is sensitive to relatively weak external forces and does not require the addition of new magma. However, the thermal engine that ultimately drives the CF hydrothermal-magmatic supersystem should not be neglected. Indeed, since the pioneering work by De Vivo and Lima (2006) up to the most recent study by Lima et al. (2025a, and reference therein), it was shown that the ultimate heat engine that drives bradyseism at CF must be the deep magmatic system at > 7.5 km depth. The extent of fracturing does not represent competition between fluid escape and injection rates because the release of magmatic fluid and upward transport of magmatic heat is continuous over time. Instead, the differential expansion of rock and pore fluid due to heating gives rise to poroelastic effects (Detournay and Cheng, 1993) including fluid migration and fracture propagation. Without the thermal effects of the magmatic engine these effects would not occur.

The aim of this study is to assess whether and how rainwater infiltration on interannual to multidecadal timescales contributes to bradyseism in the CF. To achieve this goal, we developed a schematic-conceptual model to simulate groundwater recharge as a function of the local precipitation record and its hypothesized discharge to the sea. For this reason, it was also necessary to reconstruct the CF stratigraphic and structural architecture to highlight the impermeable and permeable units along with their distribution within the CF system. More specifically, first we constructed a schematic hydrological model related to the complex stratigraphy underlying the CF area and identified the recharge areas in CF in relationship to areas experiencing seismic activity and bradyseism. Then, we adopted a realistic — albeit simplified — hydrogeological model to dynamically evaluate the recharge level of the reservoir beneath Pozzuoli and its temporal variation in response to the local rainfall record since 1950. An inverse approach, required by the hydrological model, is adopted to determine the hydraulic conductivity of the reconstructed strata in the CF area. Developing a physics-based reductionist approach in which all known physical processes are considered to compute the output is impractical due to the excessive number of unknowns.

2. Overview and history of bradyseism in the Campi Flegrei volcanic system

2.1. Geologic framework of the CF area

The CF volcanic system is located along the coast of the Campanian Plain, on the eastern margin of the Tyrrhenian Sea where the most recent back-arc extensional basins developed (Fig. 1a).

Some authors have attempted to reconstruct the CF stratigraphic pattern through seismic tomography and magnetotelluric data interpretation (e.g., De Landro et al., 2025; Isaia et al., 2025); however, in our view, such data remain insufficient to provide a detailed understanding of the area's stratigraphic and tectonic architecture. Reconstruction of the stratigraphic architecture and the structural framework is a fundamental first step to constrain the lateral and vertical extents of impermeable strata, and the permeability characteristics of the various stratigraphic units. To achieve this goal, because CF stratigraphy is the result of the interplay between tectonics, sediment supply and volcanic activity, we consider the evolution of the Campanian Margin

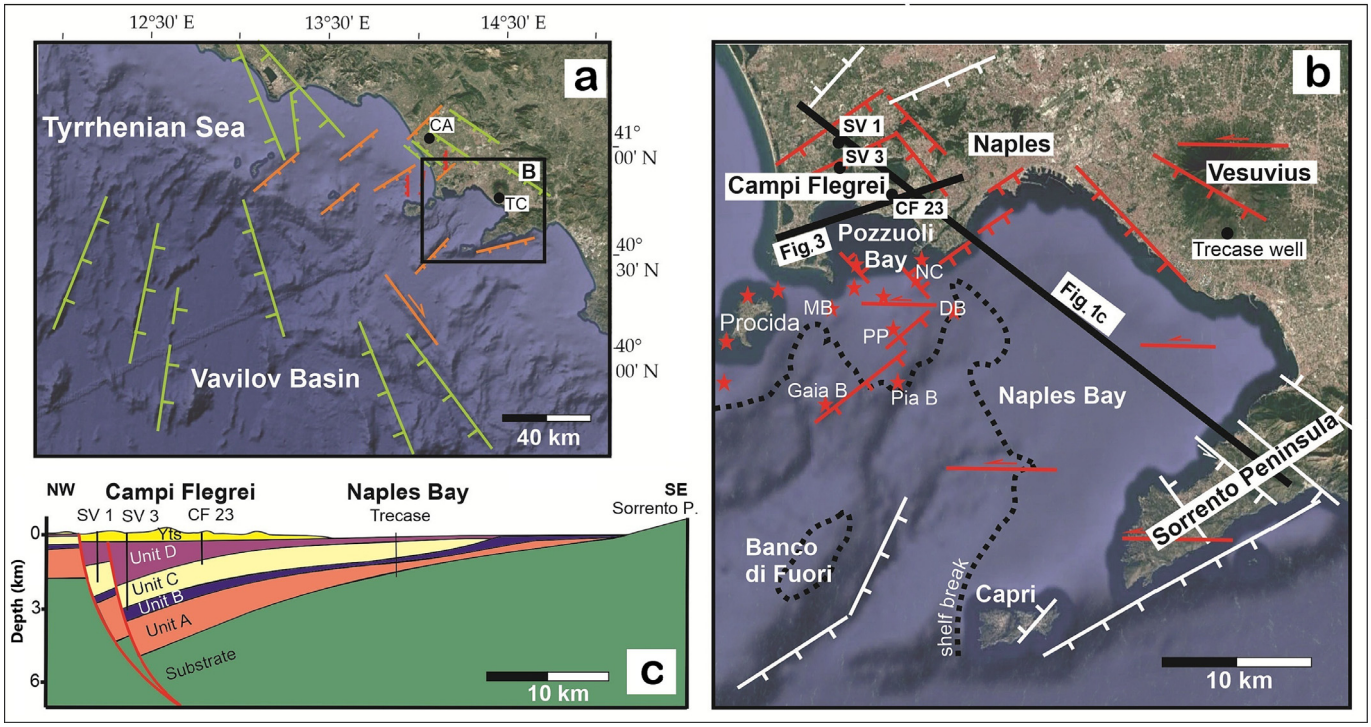

Fig. 1. (a) Structural map of the Vavilov Basin-Eastern Tyrrhenian Margin; the green faults are Pliocene in age in the Central Tyrrhenian Sea and Lower Pleistocene in the Eastern Tyrrhenian Margin, the orange faults are Middle Pleistocene. CA: Cancello borehole; TC: Trecase borehole. Modified from Milia and Torrente (2015a,b). (b) Structural map of the Campanian Margin from the Sorrento Peninsula to the Campi Flegrei area. White faults are Middle Pleistocene in age; Red faults are Late Quaternary in age (PP: Penta Palummo; MB: Miseno Bank; DB: Monte Dolce dike; NC: Nisida Complex). Modified from Milia and Torrente (2011). (c) NW-SE geologic section across the Campanian Margin that shows the stratigraphy of the Naples Bay-Campi Flegrei half-graben bounded by the Middle Pleistocene-late Quaternary NE-SW trending normal faults (Modified from Milia et al., 2003; Milia and Torrente, 2011, 2020).

(Fig. 1b) starting from the Lower Pleistocene when the first clastic sediments covered the Meso-Cenozoic substrate. In particular, three first-order tectonic events took place during this period (Milia and Torrente, 2020).

The earliest tectonic event is represented by the eastward opening of the Vavilov back-arc basin (Fig. 1a). The initial event led to the formation of the Lower Pleistocene NW-trending normal faults, which affected the exposed Apennine chain, and created symmetrical basins (e.g., the Sorrento graben; Milia and Torrente, 1997). Unit A (Fig. 1c), consisting of a sedimentary succession ranging from continental to shallow marine environments, was deposited during this stage (Milia and Torrente, 1999, 2015a, 2015b; Milia et al., 2003). These deposits, dated to 1 Ma, have been documented in the Trecase and Cancello boreholes, located northwest and southeast of the CF, respectively, and in outcrops along the margin of the Campanian Plain (Bernasconi et al., 1981; Brocchini et al., 2001; Milia and Torrente, 2015a, 2015b; Cerrone et al., 2021).

The second tectonic event corresponds to the extension toward the southeast of the Campanian Margin. This event led to the formation of Middle Pleistocene NE-trending normal faults, generating asymmetric grabens — most notably the Naples Bay–CF half graben (Fig. 1c). During this stage, Unit B (0.7 – 0.4 Ma) was deposited. This period marked both the uplift of the Sorrento Peninsula and the rapid subsidence of the CF basin, corresponding to the deposition of a relatively thin strata of deep-water environment sediments (Milia and Torrente, 1999). These deposits (Unit B, Fig. 1c) consist of clay-rich lithologies forming a transgressive unit that blankets the basin and were identified in the Trecase, Mofete, and S. Vito boreholes (Rosi and Sbrana, 1987; Brocchini et al., 2001; Marini et al., 2025). Subsequently, the half graben was infilled by a thick regressive unit — Unit C (Milia, and Torrente, 1999) — made up of three substantial lowstand prograding wedges. Unit C (Fig. 1c), dated between approximately 0.4 Ma and 0.1 Ma, consists of silt, sand, and conglomerate. During this phase, numerous volcanic products, primarily composed of lava, were interlayered within the stratigraphic succession. These have been documented in the Trecase borehole (Brocchini et al., 2001), in the southern Gaeta Bay offshore region and in the Mofete boreholes (Rosi and Sbrana, 1987), and in the Penta Palummo (PP) area shown in Fig. 1b (Milia et al., 2006).

The third tectonic event relates to a change in the direction of extension along the margin towards the east-southeast (Fig. 1a, 1b). This event, which shaped the current structural configuration, occurred over the past 0.1 Ma and is associated with major ignimbrite eruptions along the Campanian Margin (De Vivo et al, 2001; Rolandi et al., 2003). For the first time, the continental shelf of Naples Bay and the Campanian Plain recorded simultaneous activity of normal faulting and ignimbrite volcanism (Milia, 2000; De Vivo et al., 2001; Torrente et al., 2010). As a result of this tectonic event, pre-existing NW–SE trending normal faults were reactivated, and thick ignimbrite wedges accumulated along the Campanian Margin – Unit D in Fig. 1c (Milia and Torrente, 2011, 2020). In the last 14 ka (post-Neapolitan Yellow Tuff), an intricate fault system developed, producing localized transpressional tectonics. This tectonic style led to a local compression within the CF area and the formation of a detachment fold, whose anticline culminates beneath the city of Pozzuoli (Fig. 2a; Milia and Torrente, 2000). The folding extends from the Epitaffio Valley, west of Pozzuoli, to the Bagnoli area (Milia et al., 2000; Milia and Giordano, 2002). Fig. 2c illustrates the eastern flank of the syncline and Fig. 2d shows the faulted and folded strata offshore the city of Pozzuoli. The Solfatara volcano (ca. 4 ka) (Fig. 2b), located on the crest of the anticline, is a maar/diatreme structure that formed through phreato-magmatic processes, with faults extending to

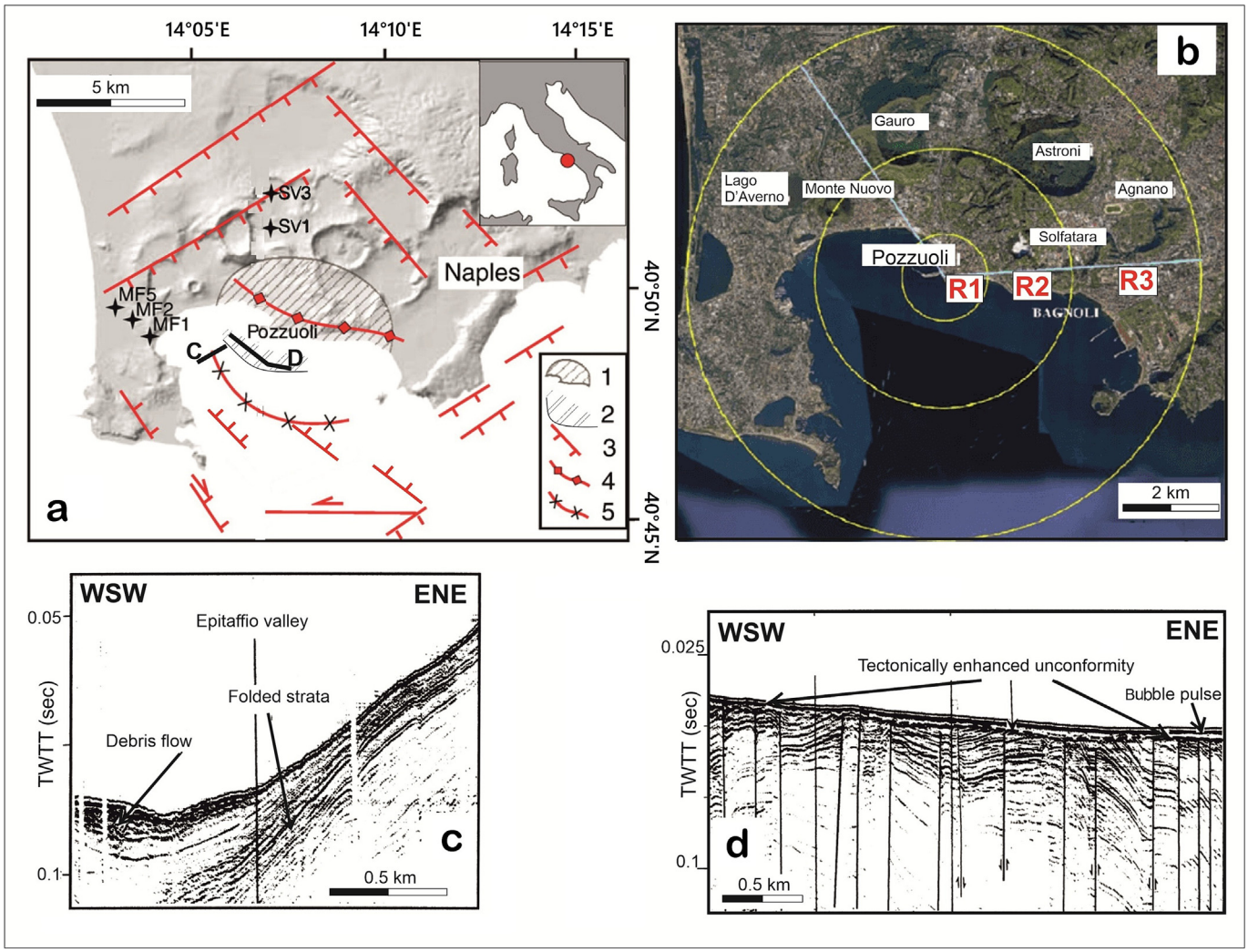

Fig. 2. (a) Structural map of the Campi Flegrei–Pozzuoli Bay area (from Milia and Torrente, 2000): 1. Onshore; 2. Offshore, highly fractured areas (affected by an uplift of 100%–50%); 3. Normal faults; 4. Crest of the Pozzuoli anticline; 5. Trough of the Pozzuoli syncline. Black stars indicate the location of deep geothermal boreholes (Mofete – MF1, MF2, MF5, and San Vito – SV1, SV3). (b) Google Earth CF map showing the hypothesized three concentric buffers used in the model (R1-R2-R3) into which the CF region is conceptually divided considering the tectonic areas (red fault lines) shown in (a), which are interpreted to be characterized by different hydraulic conductivities. (c) Seismic section across the Syncline (Epitaffio Valley) offshore Pozzuoli along line C shown on Fig. 2a (modified from Milia et al., 2000). (d) Seismic section through the faulted zone offshore Pozzuoli along line D shown on Fig. 2a (modified from Milia et al., 2000).

depths of approximately 2–3 km (Cipriani et al., 2008; Marini et al., 2022). Its structural configuration can be interpreted as being linked to opening fractures/faults commonly associated with crestal anticline settings associated with a tangential-longitudinal strain mechanism (Ramsay, 1967).

2.2. Bradyseismic activity at Campi Flegrei

The penultimate period of significant volcanic activity in CF occurred between about 5500 and 3500 years ago, during which numerous eruptions took place with the formation of several eruptive centers including on the eastern side of CF at Agnano-Monte Spina, Astroni and Solfatara (Fig. 2b) (Orsi et al., 2009). In 1538 the Monte Nuovo eruption occurred; this is the only historic eruption known to have been preceded by significant ground uplift. In the years preceding the Monte Nuovo eruption about 7 m asl of ground uplift was reported (Rolandi et al., 2025) in a small area including the vent. Following the 1538 eruption, a subsidence phase began and probably persisted until 1950, at which point an uplift phase occurred from 1950 to 1952 (Rolandi et al., 2025). Subsequent uplift episodes were recorded from 1969 to 1972 and 1982 to 1984. The 1982–1984 bradyseism event, the most extensively studied, resulted in an uplift of 186 cm that was accompanied by low-magnitude seismic swarms (maximum M = 4.0), with up to 610 seismic events occurring within a few hours (Del Gaudio et al., 2010). After 1984, a period of subsidence ensued, lasting approximately 20 years at an average rate of ~ 4 cm/year, culminating in a total subsidence of ~ 93 cm. During this subsidence phase, short episodes of mini uplift, lasting a few months, were observed in 1989, 1994, 2000, and again during 2012–2013, coinciding with the slow uplift phase that began in 2005 (Fig. 3) (Orsi, 2022). This accelerating uplift phase, ongoing to the present day, is a source of concern due to intensified seismic activity, including a M = 4.6 event that occurred on March 13, 2025, at a depth of 2.5 km below the seafloor in front of "*Località la Pietra*" in Bagnoli and east of Solfatara along the main fault (Figs. 2 and 4). The *Osservatorio Vesuviano – Istituto Nazionale di Geofisica e Vulcanologia* (OV-INGV) reported that the waveform for the latter event consists of two earthquake signals whose first arrivals occur in very rapid sequence (OV-INGV Surveillance Bulletins, March 2025). In addition, increasing fluid emission and fumarolic tremor amplitude, which is indicative of hydrothermal activity, were reg-

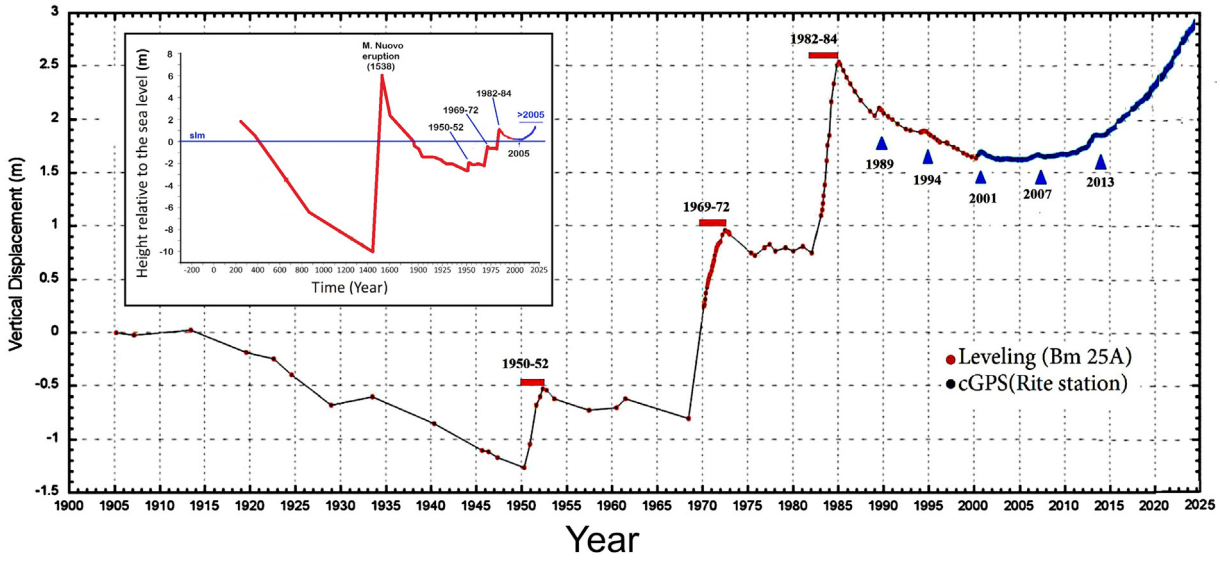

Fig. 3. Ground displacement at Pozzuoli Porto since 1905, measured by precision leveling (until year 2000, in red) and using data from the nearby GPS benchmark of Rione Terra (since 2000, blue dots) (from the Bulletins of the Osservatorio Vesuviano, INGV and Bevilacqua et al., 2024). (Inset) Reconstruction of the vertical displacement of the Serapeo fourth floor in Pozzuoli, from the 3rd century CE to the present (Rolandi et al., 2025).

istered along with uplift of about 1.5 m from January 2005 to September 2025 in the Pozzuoli area (cf. Chiodini et al., 2017).

2.3. A model to explain CF bradyseism

The hydrothermal model to describe bradyseism and ground deformation at CF is based on research by the current authors over the past several decades and summarized by De Vivo and Lima (2006), Bodnar et al. (2007), De Vivo et al. (2009), Cannatelli et al. (2020), and Lima et al. (2009, 2021, 2025a). Our model proposes that the fundamental driver of bradyseism at CF is the magmatic system located at depths greater than 7.5 km (Fig. 4). During crystallization, the magma becomes volatile (H_2O, CO_2) saturated and releases magmatic fluid that accumulates beneath an impermeable cap that occasionally fractures, allowing the magmatic fluids to migrate upwards. Upward migrating magmatic fluids accumulate in Unit A beneath the impermeable Unit B (Fig. 4), which episodically fractures in response to the increased fluid pressure and allows magmatic fluids to migrate upward into Unit C, which also acts as a fluid reservoir. Here, magmatic fluids mix with marine and meteoric water (Caprarelli et al., 1997; Calìro et al., 2025). Bradyseism is primarily driven by the transient connection between reservoirs hosted in Units A and C, mediated by impermeable Unit B. Recently, Mantiloni et al. (2025) validated their analytical poroelastic solutions with Finite Element models, then used them as initial conditions to study surface displacement and pore pressure/stress changes from fluid flow between porous layers with different regimes. The episodic connection and disconnection between deeper and shallow reservoirs are sufficient to drive the 'breathing' mode. In Lima et al. (2025a and references therein) model, two processes operate on distinct and different timescales. The longer timescale, on the order of 10^3–10^5 years, is associated with magma cooling, solidification and production of lithostatically-pressured fluids, during which the brittle-ductile transition migrates to greater depths (see fig. 3 in Lima et al., 2025b). The shorter timescale, ranging from 1 to 10^2 years, is episodic in nature and linked to fluid migration and transient fracture propagation aided by increasing effective stress within the impermeable Unit B. Ground deformation and seismicity are thus driven by fluid pressurization in the underlying reservoir leading to uplift, with subsidence caused by fluid depressurization following brittle failure and enhanced fracture permeability that allows the trapped overpressured fluids to escape and migrate upwards. The closing of the system occurs mostly by mineral deposition and relaxation after pressure release that closes the fractures and locally decreases permeability. So far, no model, including one recently proposed by Vanorio et al., 2025, has been able to explain the so-called mini events (Fig. 3) represented by interannual fluctuations that occur both during the multidecadal subsidence and uplift phases. An explanation of these neglected mini-events is one of the goals of this study: the correlation of these mini-events with the record of rainfall and aquifer recharge.

3. Subsurface geology at CF: Origin of the earthquakes and fluid circulation

A fundamental step for reconstructing the fluid circulation in the CF region consists in characterizing the location and lateral extent of the relatively permeable and impermeable stratigraphic successions and the structures, folds and faults, in the area of interest. The east–west geological section across the CF region (Fig. 4) allows the identification of the main geological units that characterize the area, which are described below from bottom to top. A melting zone, affecting both the crystalline basement and the carbonates of the faulted Apennine thrust belt units (indicated as the substrate in Figs. 1c and 4) is covered by an irregular impermeable zone (carapace), formed by crystallized magma.

The substrate is covered by Unit A. The lower boundary of Unit A is an irregular surface, with a shape similar to the top of the carbonate unit outcropping along the Sorrento Peninsula, as confirmed by tomographic data showing seismic velocities exceeding 5 km/s at approximately 4 km depth (De Landro et al., 2025). Indeed, the thickness of Unit A is controlled by the Lower Pleistocene faults, forming a graben in the central part of CF, as shown in Fig. 4a. This structure corresponds to the NW-oriented grabens, such as those that crop out on the Sorrento Peninsula and the one that is buried in the northern Campanian Plain (Fig. 1). Unit A consists of continental and shallow-water sedimentary deposits that reach a thickness of 1.5 km based on Trecase and Cancello boreholes and is comprised of a succession of sands and silts interlay-

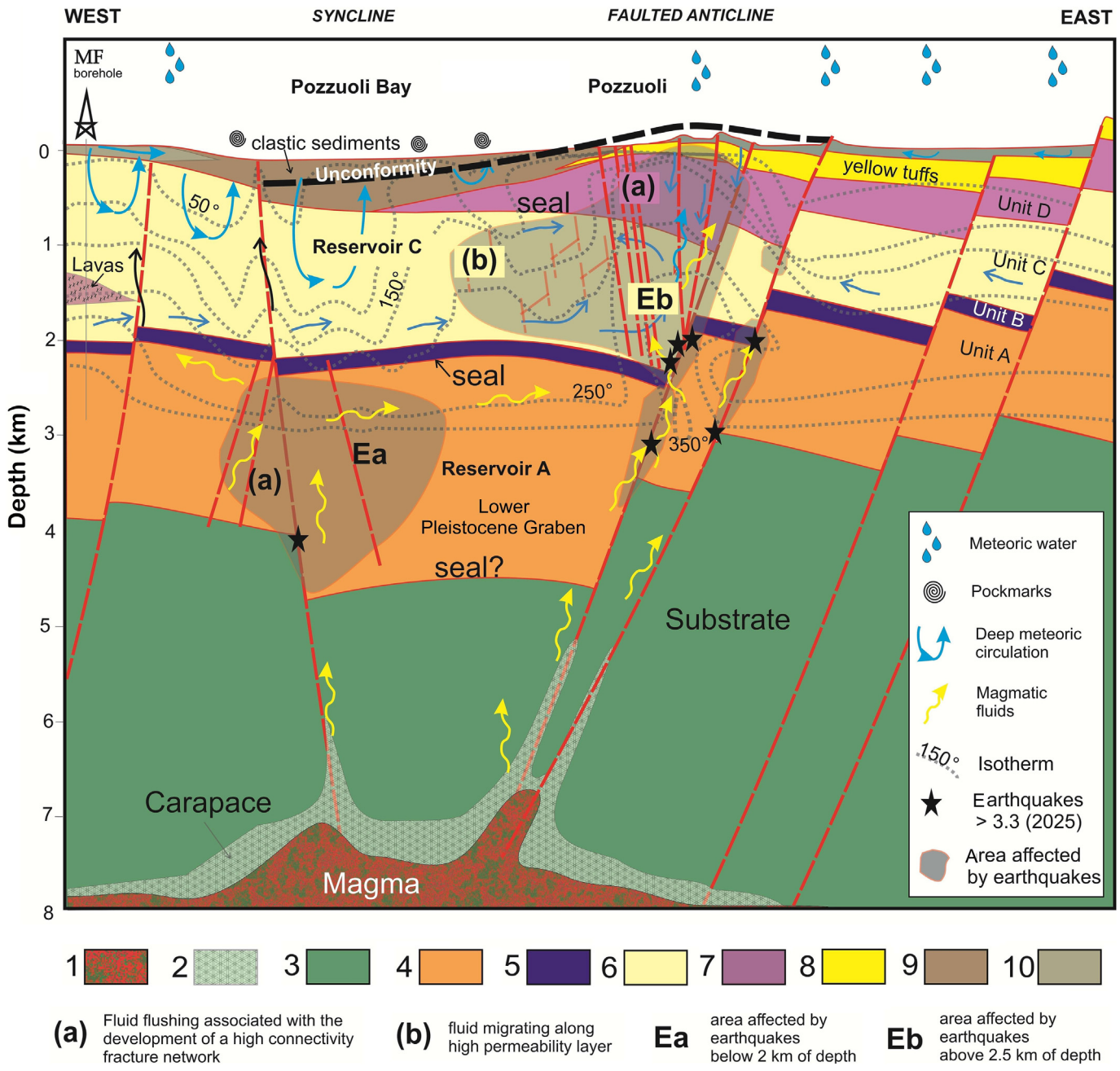

Fig. 4. Schematic migration pathways for both meteoric and deep magmatic fluids. Fluids in the reservoir Unit C are confined by the Unit D that thins out and disappears beneath the Gulf of Pozzuoli, where fluids can migrate up to the seafloor surface to produce the observed pockmarks. E-W oriented geologic section across the Solfatara-Pozzuoli area and Pozzuoli Bay (for location see Fig. 1a). The various geologic and stratigraphic features shown include faults and fractures in red. Color legend: (1) Magma depth (Zollo et al., 2008); (2) Crystallized magma (Lima et al., 2025a and references therein); (3) Crystalline/carbonate lithologies; (4) Unit A (1.0–0.7 Ma), made up of continental to shallow marine deposits, representing the deeper reservoir of magmatic fluids (Milia and Torrente, 2015a, 2015b; Lima et al., 2025a and references therein); (5) Unit B (0.7–0.4 Ma), mainly made up of clays representing the deeper impermeable unit; (6) Unit C (0.4–0.1 Ma), made up of silts and sands with localized old lava lenses, representing the shallow reservoir containing mostly meteoric and sea waters; (7) Pyroclastic deposits including the Campanian Ignimbrite deposits (Unit D, < 0.1 Ma) representing a relatively impermeable unit compared to overlying and underlying units, this Unit D is highly permeable where highly fractured and faulted; (8) Yellow Tuff deposits (<35 ka); (9) Marine clastic sediments (silts and sands) in Pozzuoli Bay, the unconformity marks the boundary between the pre-folding strata and *syn*-folding deposits; (10) Alluvial deposits onshore.

ered by conglomerates and mudstone and acts as a permeable fluid reservoir (Fig. 4b).

A relatively thin clay-rich Unit B lies above Unit A, forming an impermeable unit with a large regional extent. Seismic lines located on the eastern margin of the Penta Palummo (PP, Fig. 1b) area support this interpretation. Fig. 5b shows a north–south multichannel seismic reflection profile that crosses an area where the pyroclastic deposits are absent (Fig. 5a). The interpretation of the profile, based on cross-correlation of densely spaced seismic profiles acquired in Naples Bay (e.g. Milia and Torrente, 2011), reveals a high amplitude, low frequency and continuous reflector corresponding to Unit B, between Unit A and the overlying Unit C. The seismic section (Fig. 5b) shows continuous parallel reflectors for Unit C, whereas Unit A is marked by continuous parallel reflectors in the southern part and by scattered high-amplitude reflectors towards the north. This latter seismic facies suggests the presence

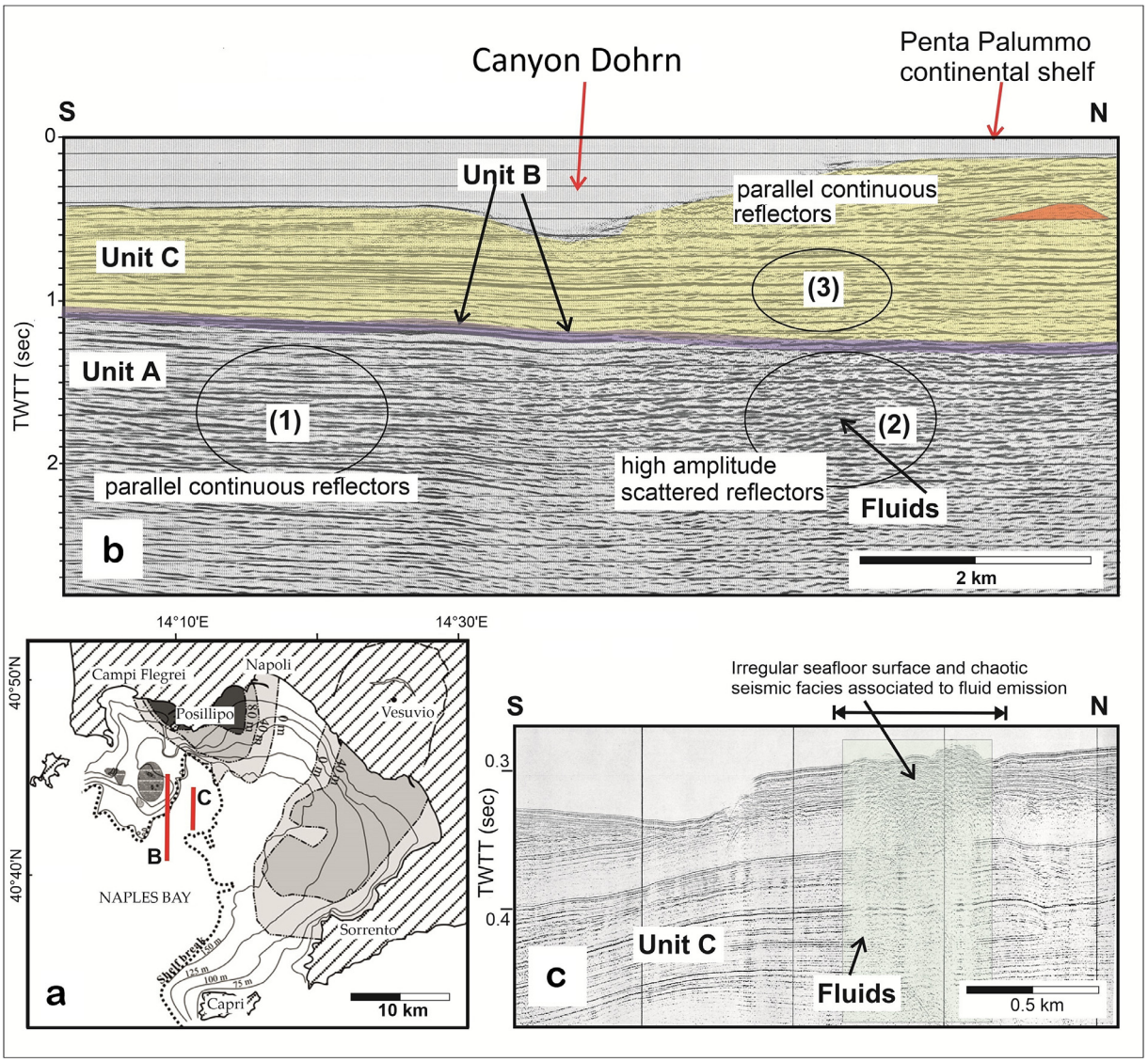

Fig. 5. N-S oriented seismic sections supporting the interpretation of fluid pathway in the stratigraphic succession offshore Campi Flegrei. (a) Map showing the distribution of the Campanian Ignimbrite and location of the seismic profiles shown in (b) and (c). (b) Multichannel seismic section showing Unit A characterized by parallel reflectors (1) that transitions to a high amplitude scattered reflections northward (2), indicating the presence of fluids in the sediments below Penta Palummo area. Upward the Unit C, is characterized by parallel reflectors (3) from North to South. The change of the seismic facies from (2) to (3) indicates that Unit B corresponds to an impermeable seal. (c) Single channel seismic reflection profile showing evidence for the migration of fluids, that are present in the Unit C, until the seafloor in the area where the pyroclastic units are absent.

of fluids in the sediments. Since these facies are confined to Unit A, it demonstrates that Unit A is a fluid reservoir sealed by Unit B which prevents the upward migration of the fluids. This interpretation is supported by the findings in the Mofete 5 borehole that identified two aquifers at depths of 1600–1960 m and 2310–2699 m, separated by the impermeable layer corresponding to Unit B (Mf5, Figs. 2a and 4) and by the presence of an aquifer in the CF23 borehole at depths of 1445–1712 m (Fig. 4; Carella and Guglieminetti, 1983; AGIP, 1987).

Unit C is a regressive marine succession composed mainly of silts and sands, with interbedded lavas and volcanic deposits related to the earliest volcanism along the Campanian Margin. Due to its lithological characteristics, Unit C corresponds to a relative permeable unit (Reservoir C, Fig. 4).

A relatively thick pyroclastic unit, Unit D, overlies Unit C in the Pozzuoli area and corresponds to the pyroclastic, ignimbrites and volcanoclastics deposited over the last 100 ka (e.g. Milia and Torrente, 2011). This unit is characterized by low permeability due to welding, grain size variability, and post-depositional alteration and mineralization and can be considered a relatively impermeable unit. The pyroclastic unit presents a wedge external form, thickening toward the north, where it reaches a depth of approximately 2.5 km in the S. Vito borehole (Fig. 1c), and pinches out toward the west (Fig. 4). It is important to note that the lower boundary of the pyroclastic Unit D varies from about 2.5 km in the San Vito borehole to about 1 km below Pozzuoli, to about 0.5 km in the middle of Pozzuoli Bay, and disappears (or is present only in thicknesses of a few meters or as tephra) west of Pozzuoli (Milia and Torrente, 2011). Consequently, Reservoir C is only bounded upward by an impermeable unit where the pyroclastic wedge is present, thus representing a localized reservoir. This wedge architecture and the deepening of the base toward the faults (Fig. 1c) reflects the late Quaternary *syn*-ignimbrite fault activity (Milia, 2000; Milia and Torrente, 2011). The uppermost

part of the succession comprises the younger Neapolitan Yellow Tuff deposits and alluvial sediments onshore, and marine silts and sands in Pozzuoli Bay (Fig. 4).

In areas where Unit D is absent, fluids circulating in Unit C can migrate upward to the sea floor, forming pockmarks as shown in Figs. 4 and 5c. The seismic section of Fig. 5c illustrates vertical features with transparent facies at depth terminating at the seafloor as chaotic facies and irregular topography, these features are characteristic of fluid migration pathways.

From the tectonic point of view, over the last 8 ka the CF/Pozzuoli Bay area has been characterized by active tectonics. In particular, the architecture of the sedimentary succession revealed a major fold, with an anticlinal culmination beneath Pozzuoli and a syncline beneath Pozzuoli Bay, formed in response to a local transpressive deformation (Milia and Torrente, 2000, 2003). The folding reflects positive inversion tectonics due to the reactivation of pre-existing normal faults. During tangential-longitudinal strain folding, extensional faults and fractures form along the anticline crest and syncline troughs to accommodate the tectonic deformation (Figs. 2d, 6b; Ramsay, 1967).

The Solfatara structure is a maar/diatreme system formed during a phreatic eruption ~ 4 ka ago, with faulting extending to ~ 2 km depth (Cipriani et al., 2008; Marini et al., 2022). This area exhibits intense faulting aligned with regional tectonic trends (e.g. Bruno et al., 2007). The highly fractured zone between Solfatara and Pozzuoli, particularly the diatreme itself, can be interpreted as a crestal collapsed structure atop the anticline (Figs. 4 and 6c).

The distribution of earthquakes is consistent with the reconstructed structure. Indeed, the earthquakes are concentrated at about 1–2 km depth beneath the anticline, while deeper events off-

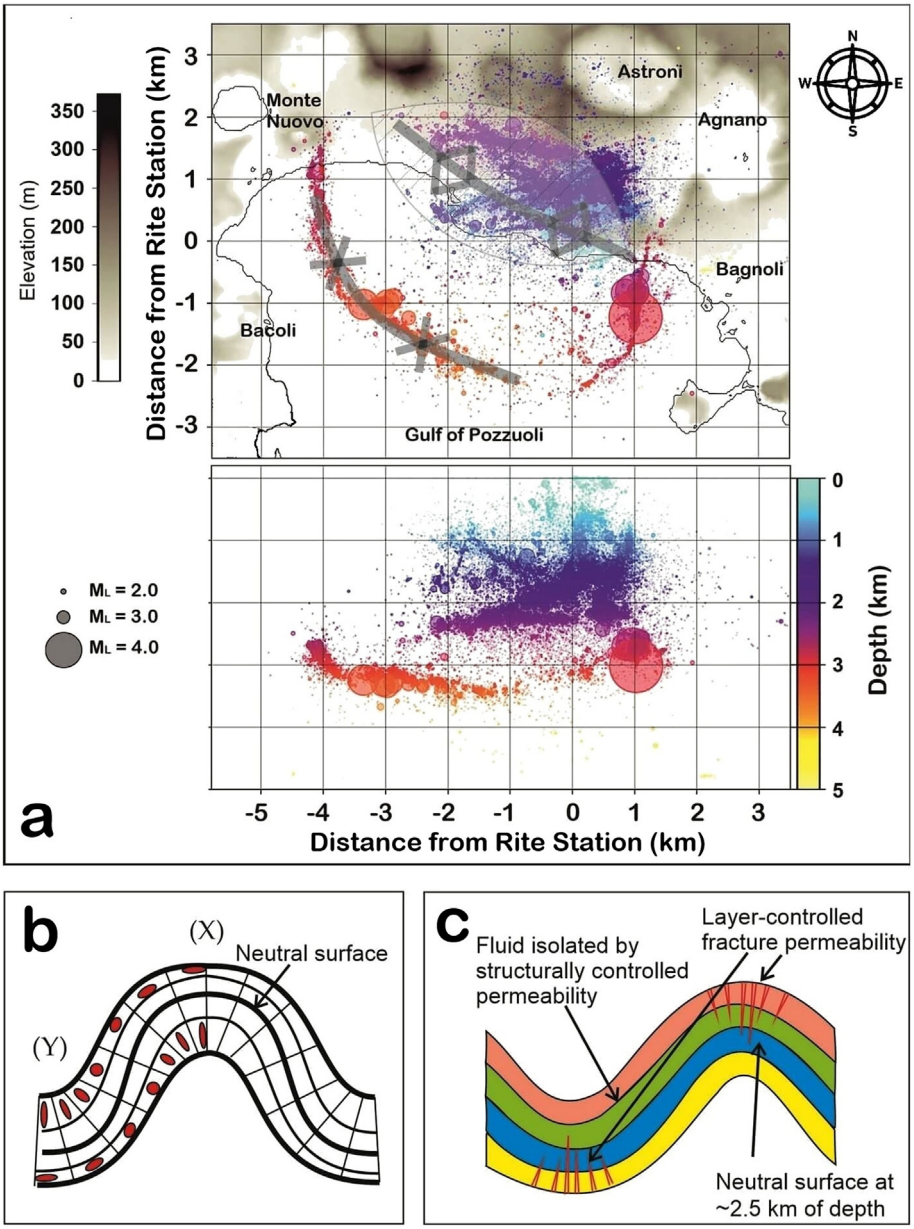

Fig. 6. (a) Relocated seismicity 2014–2023 — its surface distribution and vertical projections along the XY axes — in the Campi Flegrei area (redrawn from Tan et al., 2025), also shown are the traces of the syncline and anticline axes of Fig. 2a. The reference point is Rite Station (14.14°E, 40.82°N). (b) Strain distribution within a fold showing extension in correspondence of the anticline (X) and of the syncline (Y) respectively above and below the neutral surface (from Ramsay, 1967). (c) Structural and stratigraphic compartmentalization showing that as the permeability is strictly controlled by the fractures and strata permeability. The comparison with the Pozzuoli Anticline and the depth of earthquakes suggests a neutral surface at 2/2.5 km of depth.

shore lie between 2–4 km beneath the syncline (Figs. 4 and 6a) (cf. Tan et al., 2025). Seismicity is linked to ongoing folding, with fractures developing both above and below the neutral surface of the fold (Fig. 6b and 6c) (Ramsay, 1967) and in association with tectonic faults. Numerous micro-earthquakes affect the area (Fig. 6) especially in the intermediate zone between the anticline and syncline between depths of 1–2 km and upward in the Pozzuoli/Solfatara area. These micro-earthquakes can be attributed to the fractures generated by the fluid overpressure in Reservoir C and in the hinge zone of the anticline. Furthermore, according to the development of an inversion tectonic structure in a local transpressive regime, the focal mechanisms show transcurrent and oblique motion along faults-oriented NW, SE, NE, SW, EW, and NS, and the coexistence of both normal and reverse faulting (Milia and Torrente, 2003; Natale et al., 2024; Tan et al., 2025).

The reconstruction of stratigraphic and structural features, as illustrated in the geologic section shown in Fig. 4, is used for reconstructing the fluid circulation system, as illustrated in Fig. 4b. From the stratigraphic perspective, we can identify two relatively first-order impermeable levels: (1) Unit B, extending over the entire Campanian Margin at a depth of approximately 2 km in the Pozzuoli area; and (2) the pyroclastic units (Unit D), with a limited extension, at a depth of 0.5–1 km in the Pozzuoli area and thins to the west and terminates in Pozzuoli Bay. Two thick reservoirs are present between the impermeable units. Under Pozzuoli city, Unit A represents the reservoir for the fluids released from the deeper crystallizing magma and is separated from overlying units by impermeable Unit B. Unit A is subject to overpressure conditions until Unit B fractures, allowing fluids to escape upwards (Lima et al., 2025a, and references therein). The shallower Unit C represents a meteoric fluid reservoir and is present only where it is overlain by the pyroclastic wedge. A large-scale fracture permeability affects the area and allows fluids from Reservoir A to migrate upwards to Reservoir C, where the fluids mix and eventually escape to the surface in the Solfatara/Pisciarelli area along localized tectonic faults.

The reconstructed water circulation model (Fig. 4b) indicates that meteoric water falling on the CF accumulates under the Pozzuoli-Solfatara area. On the western side, under Pozzuoli Bay, sea water mixes with underground fluids, migrating both laterally and vertically, forming pockmarks on the flanks of the syncline in Pozzuoli Bay where the fluids reach the seafloor (Fig. 4). Mixed fluids (meteoric, marine, and magmatic) from different depths migrate upward through the fractures at Solfatara, as reported by several studies (Caprarelli et al., 1997; Calìro et al., 2025). The fluid circulation pattern illustrated in Fig. 4b is consistent with the isotherm reconstruction proposed by Petrillo et al. (2013). In the western portion of the section, the isotherms descend into the basin, indicating lower temperatures compared to the eastern sector near the Pozzuoli-Solfatara area. Here, the isotherms rise, reflecting higher temperatures along the interface between Unit C and Unit B. The influx of cold meteoric fluids from inland areas into Unit C, combined with the influence of seawater in the bay, where Unit D is absent, causes the isotherms to be depressed to greater depths. Conversely, the ascent of hot fluids along major fracture zones, particularly along faults that extend to great depth near the top of the anticline, results in a sharp upward deflection of the isotherms (Fig. 4b).

4. Model to evaluate rainwater accumulation

At CF, rainwater can infiltrate into the subsurface through intense fracturing and is likely to accumulate primarily within Unit C. This accumulation increases both underground pore pressure and the pressure generated by the convective movement of hot water and pressurized water rising through the system. These pressures reduce the effective stress that binds the rocks together, potentially allowing for ground movement and uplift of the overlying surface.

The magnitude of this uplift depends on three main factors: (1) the volume of infiltrated water; (2) the compressibility and poroelastic properties of the surrounding rocks; (3) the magnitude of lithostatic confined pressure beneath the impermeable layer.

Geothermal activity can amplify the uplift through thermo-poroelastic effects. The resulting increase in pore pressure and ground deformation may induce earthquakes via two primary mechanisms: (1) When pore pressure surpasses the tensile strength of the rock, new fractures can form, releasing stress suddenly and generating small earthquakes; (2) Elevated pore pressure can reduce frictional resistance along pre-existing faults. This process — known as fault reactivation — can destabilize critically stressed faults and cause sudden slips that trigger earthquakes, especially in zones with significant water infiltration (Casertano et al., 1976; Bonafede and Mazzanti, 1997; Siniscalchi et al., 2019; Guerriero and Mazzoli, 2021, and references therein; Wang and Manga, 2021).

Rainwater at CF discharges through surface runoff, evaporation, and underground percolation, eventually reaching the sea. Fig. 4b shows a geologic section across Campi Flegrei–Pozzuoli Bay, illustrating meteoric water circulation. It also shows the modelled subsurface path and accumulation of rainwater within Reservoir C (see section 2.1).

We hypothesize that rainwater falling more than 6 km from Rione Terra does not contribute to the aquifers beneath Pozzuoli, as it is likely diverted by the main fault encircling CF (Fig. 2a). Several highly fractured areas within CF, such as the Astroni crater (Fig. 2b and Fig. 4), may serve as major recharge areas. Tectonic or seismic activity can alter these fractures — sealing or opening them — and consequently modulate water recharge and discharge rates. A reduction in these rates leads to a change in meteoric water accumulation in Reservoir C (Fig. 4). In addition, groundwater infiltration is also influenced by variations in rainfall intensity. The seawater contribution is considered approximately constant.

The aim of our model is to determine whether interannual to multidecadal changes in rainfall amounts are correlated with the vertical surface displacements observed in the uplift zone centered around Pozzuoli (GNSS Rite Station). Detecting a correlation across multiple timescales (cf. Scafetta et al., 2004) between the uplift and rainwater accumulation would suggest that the impermeable stratum Unit D is affected by pressure changes due to: (1) vertical movement of the deeper Unit B pushed upward by inflation of Reservoir A, as already suggested in Lima et al. (2025a, and references therein); (2) expansion of Reservoir C (region Eb in Fig. 4) where meteoric water can accumulate in the region above the anticlinal structure (Fig. 6).

4.1. Inverse approach to assess the local hydraulic conductivity

The creation of a hydrogeological model requires knowledge of the hydraulic conductivity of the strata in the CF area. This knowledge is not known *a priori*. In fact, envisioning a physics-based reductionist approach in which all known physical processes are considered to compute an output, is impractical due to the excessive number of unknowns.

The conversion of hydraulic conductivity (K) to the intrinsic permeability (k), a property of the rock matrix independent of the fluid properties and dynamics, depends on the saturation level of the medium as well as the dynamic viscosity and density of the fluid occupying the pore (or fracture) network. For a fluid saturated medium $[MICK] = \frac{\rho \vec{g}}{\eta} k$. For water near the surface, the factor converting intrinsic permeability to the hydraulic conductivity is ≈

9.1×10^{-8} . However, under more realistic hydrothermal conditions, for example 350 °C and about 70 MPa (700 bars) at a depth ~ 3 km, the ratio $\frac{\eta}{\rho}$ is a factor of 7 larger compared to shallow groundwater. However, in our case, the lithology of the area is highly fractured and, therefore, it is not possible to derive the hydraulic conductivity from general hydrothermal conditions. Hence the use of hydraulic conductivity provides a mean-field description that includes variations in fluid properties and medium anisotropy and heterogeneity (e.g., dependence of k on depth and lithology), which could be eventually used to find an effective intrinsic permeability (Bear, 1972).

The construction of an empirically based hydrogeological model starts by examining the data. It is observed that both the rainfall record and the ground vertical displacement record exhibit significant interannual fluctuations that appear to be correlated with a time lag of a few years. Based on this observation, it is hypothesized that rainwater falling on CF infiltrates in an underground core reservoir located under Pozzuoli and affects the vertical movement. Since the hydraulic conductivity of the ground is a free parameter of our model, the hydraulic conductivity value is randomly varied within a range of values that the literature considers realistic for highly fractured igneous and metamorphic rocks (Freeze and Cherry, 1979) until a reasonable single value is found that could replicate the observed time lag between the interannual fluctuation observed in the rainfall record and in the ground vertical displacement record. We notice that the hydraulic conductivity, which is a velocity, depends on other parameters such as the intrinsic permeability, the viscosity, the fluid density and the temperature. However, for our purpose we ignore this complexity and simply estimate a reasonable hydraulic conductivity derived empirically from the observations.

In this way, the modeling automatically accounts for the observed time lag between rainfall and underground recharge, as water percolates through fractured upper crust of variable lithology to reach the reservoir under Pozzuoli. This enables a comparison between the rainfall record and the vertical ground movement in Pozzuoli since 1985, allowing us to examine whether the small interannual fluctuations (mini ups and downs), along with decadal and longer modulations of the two signals, can be correlated.

A double correlation observed at both interannual and longer time scales provides stronger evidence that rainwater contributes to vertical ground movement, offering in addition a reasonable quantitative estimate — at least a lower bound — of this contribution and shedding light on the possible dynamics of the process. With the help of the model, it is possible to show that the higher limit depends on the drainage time scale of groundwater from the core reservoir (in Unit C) to the sea (Fig. 4).

4.2. Rainfall data

The proposed model uses the average daily precipitation dataset from ERA5 (Hersbach et al., 2020) to estimate rainfall over the CF region. Specifically, we sourced the daily dataset of rainfall reported in mm/day labeled "ERA5 1950-now 0.25° Europe" from the KNMI Climate Explorer (available at https://climexp.knmi.nl/, accessed on April 8, 2025). The ERA5 precipitation records are estimated averages provided on a 0.25° × 0.25° grid. Consequently, we focused on the area bounded by longitudes 13.875°E – 14.375°E and latitudes 40.625°N – 41.125°N, centered at 14.125°E – 40.875°N. This selected region closely encompasses Rione Terra in Pozzuoli (approximately 14.12°E, 40.82°N), the site of the GNSS station Rite operated by the OV-INGV. Notably, this location corresponds to the CF area of maximum ground deformation and uplift.

The data of vertical displacements at GNSS Rite Station located in Rione Terra in Pozzuoli and depicted in Fig. 3 are taken from the Bulletins of the OV-INGV (https://www.ov.ingv.it/index.php/monitoraggio-e-infrastrutture/bollettini-tutti/boll-sett-flegrei) and from the supplementary information of Bevilacqua et al. (2024).

4.3. Model

This section presents a mathematical framework for a hydrogeological model describing the dynamics of the underground rainwater percolation system beneath CF (Fig. 4). For this purpose, the surface inside the CF area has been divided into three concentric areas (Fig. 2b). We did not consider regional contributions because the tectonic structure of the CF caldera should be mostly bypassed by external flows (Fig. 2a). The model postulates that the vertical displacement observed at Rite Station, which is the area with the highest unrest, situated in Rione Terra, results from two distinct components:

$$H_{B+C}(t) = H_B(t) + H_C(t) \quad (1)$$

where $H_B(t)$ represents the vertical displacement of the deeper Unit B, located approximately 2 km below the surface, and $H_C(t)$ denotes the vertical enlargement of the more superficial Unit C, situated at a depth of approximately 1–2 km between Unit B and the impermeable Unit D. Unit B plays two roles in this process. On the one hand, it prevents deeper fluids from Unit A from continuously rising upwards to more shallow depths, and on the other hand it prevents meteoric water from migrating downward into the deeper parts of the CF system.

The expansion of Unit C is primarily attributed to meteoric water accumulation, which predominantly varies with the volume of meteoric water falling over the CF region minus the discharge. Conversely, the vertical displacement of Unit B is assumed to be influenced by variations in the deep lithostatic pressure as explained by the magmatic hydrothermal model of Lima et al. (2025a, and references therein).

The schematic model presented below integrates the influences of precipitation, percolation, and flow dynamics within a hypothesized system of concentric buffers centered at Rione Terra, the point of maximum surface uplift in Pozzuoli (Fig. 2a and 2b). These processes are hypothesized to modulate $H_C(t)$. Note that $H_B(t)$ cannot be independently quantified by our model, as the factors driving its dynamics remain unknown. Likely, $H_C(t)$ mostly determines the low amplitude and high frequency component of $H_{B+C}(t)$, whereas $H_B(t)$ may be responsible for the high amplitude and low frequency component of the vertical displacement observed at Rite Station (Rione Terra, Pozzuoli). However, some couplings may also be possible. Consequently, we infer various scenarios by analyzing and comparing the dynamical patterns of vertical displacements recorded at the Rite Station alongside variations in water accumulation developing in Unit C, estimated through rainwater amount changes resulting from variations in precipitation temporal patterns.

The region is conceptually divided into three concentric buffers, defined by radii R_0, R_1 and R_2, by taking into consideration only the land portion side (Fig. 2b).

Thus, the proposed model speculates three ideal buffers derived from the CF tectonic geometry and its faults (Figs. 2a and 4) that regulate the meteoric water infiltration falling on the region. This geometry is inspired by the observation that (1) the CF area has a radius of about 6 km from Pozzuoli (second buffer), (2) the vertical ground movement is maximum around Pozzuoli in the center of the circles shown in Fig. 2b (model core) and (3) that the maximum fracturing of the ground occurs within 3 km from Pozzuoli (first buffer) where the highest seismic activity occurs (Figs. 2a

and 6a). We verified that the model's results are not significantly influenced by these assumptions.

- **Model core:** This core is assumed to be located beneath Rione Terra at a depth h between 1 and 2 km and with a radius of $R_0 = 1$ km. This core receives most of the meteoric water falling over the area within the ring faults at 6 km radius, leading to maximum ground deformation. Water from this core can only be discharged mostly into the sea over a time scale $\tau(t)$, which varies based on the permeability by fractures that could be influenced by very slow deformation associated with local tectonic activity as previously discussed.
- **First water buffer:** The model core is surrounded by the first buffer extending to a radius $R_1 = 3$ km, including the highly fractured Solfatara area (Fig. 2b). This highly fractured area allows meteoric water to rapidly percolate and rapidly reach the model core at speed $V_1(t)$ that may vary with seismic activity.
- **Second water buffer:** This is the external buffer with a radius of $R_2 = 6$ km (Fig. 2b). This area is less fractured than the first two as we consider only the on-land portion side, resulting in a slower percolation rate, $V_2(t)$.

For this hypothesized model, it is assumed that rainfall is uniformly distributed across the entire region. The infiltration speeds $V_1(t)$ and$V_2(t)$ may change over time because the area is seismically active, and the faults may evolve by changing the rate at which the water may infiltrate. Besides this dynamic, we assume that the infiltration rates represent an average speed in each area without, for example, differentiating between horizontal and vertical movement, which are expected to be characterized by different hydraulic conductivity values. Finally, upon reaching the model core, the water can only be discharged mostly into the sea with a time scale $(\tau(t))$, which can again vary over time because of the seismic activity of the area.

4.4. Rainfall contributions

The surface areas of the three buffers where rainwater falls are:

$$\begin{aligned} A_{\text{core}} &= \pi R_0^2 \\ A_{\text{first buffer}} &= \pi R_1^2 - \pi R_0^2 \\ A_{\text{second buffer}} &= \pi R_2^2 - \pi R_1^2 \end{aligned} \tag{2}$$

Rainfall contributes to water inflow in the model core as follows.

4.4.1. Rainfall directly over the model core

Rainfall directly above the area A_{core} infiltrates vertically through the ground with a delay:

$$t_{\text{delay,core}} = \frac{h}{V_1(t)} \tag{3}$$

where h is the depth between 1 and 2 km. The daily contribution at time t to the core's water volume from this area is:

$$V_{\text{rain,core}}(t) = \frac{\alpha}{2} P(t - t_{\text{delay,core}}) \cdot A_{\text{core}} \tag{4}$$

where: $P(t)$ is the rainfall rate and A_{core} is the central area of the core (πR_0^2). The factor 1/2 is adopted because, according to the satellite photo of Fig. 2b about half of the area is covered by the sea. The assumption is completed by considering that only a fraction α generally less than 20% of the rainwater infiltrates. This fraction may vary over the entire region and, especially over the downtown area of Pozzuoli, may be rather low because the surface is mostly paved. However, in our simplified model we assume that the percolation fraction α is constant over the entire region. In this way the fraction α is just a multiplicative factor that can be normalized out. We notice that even if the rainwater contribution from the inner core, which mostly corresponds to the downtown of Pozzuoli, is ignored ($\alpha = 0$), the result of our model would change by less than 3%, because the area A_{core} is only 3% of the entire considered surface.

4.4.2. Rainfall over the first buffer

Rainfall over the first buffer area contributes to the model core through a percolation pathway, which is supposed to be linear for simplicity. The delay is:

$$t_{\text{delay,first}}(r) = \sqrt{\left(\frac{r}{V_1(t)}\right)^2 + \left(\frac{h}{V_1(t)}\right)^2} \tag{5}$$

where r is the radial distance from the center. The corresponding daily contribution at time t to the core's water volume from this area is:

$$V_{\text{rain,first}}(t) = \frac{\alpha}{2} \int_{R_0}^{R_1} P(t - t_{\text{delay,first}}(r)) \cdot 2\pi r \, dr \tag{6}$$

The factor 1/2 is again adopted because, according to the satellite photograph of the area (Fig. 2b) about half of the area is covered by the sea, and all water falling on the surface of this buffer is assumed to percolate towards the core.

4.4.3. Rainfall over the second buffer

Rainfall over the second buffer flows linearly towards the first buffer and then continues to flow towards the model core. The depth at which water reaches R_1 is:

$$h_{\text{partial}} = h \cdot \frac{r - R_1}{r} \tag{7}$$

The total delay is:

$$t_{\text{total,second}}(r) = \sqrt{\left(\frac{r-R_1}{V_2(t)}\right)^2 + \left(\frac{h_{\text{partial}}}{V_2(t)}\right)^2} + \sqrt{\left(\frac{R_1}{V_1(t)}\right)^2 + \left(\frac{h - h_{\text{partial}}}{V_1(t)}\right)^2} \tag{8}$$

The daily contribution of rainwater at time t to the model core from this area is:

$$V_{\text{rain,second}}(t) = \frac{\alpha}{2} \int_{R_1}^{R_2} P(t - t_{\text{total,second}}(r)) \cdot 4\arcsin(R_1/r) \cdot r \, dr \tag{9}$$

Eq. (9) assumes again the factor of 1/2 for the same reasons of above, but in addition it is assumed that only a portion of the meteoric water precipitating in this second area converges toward the model core. This portion decreases with the distance from the model core center as the arcsine function. Note that for $r = R_1$, $4\arcsin(R_1/r) = 2\pi$ as in Eq. (6).

4.5. Water flow dynamics

4.5.1. Total inflow to the model core

The total daily inflow to the model core is the sum of the contributions across the three regions:

$$Q_{\text{in}}(t) = V_{\text{rain,core}}(t) + V_{\text{rain,first}}(t) + V_{\text{rain,second}}(t) \tag{10}$$

4.5.2. Outflow from the model core

The daily water outflow from the model core mostly through the fractures, is proportional to its accumulated water volume as

$$Q_{\text{out}}(t) = \frac{\text{Volume}_{\text{core}}(t)}{\tau(t)} \tag{11}$$

where $\tau(t)$ is the drainage timescale. For example, when the underground water more easily percolates through fractures, τ is smaller, while when the discharge is lowered by sealing of the fractures, τ is larger.

4.5.3. Water volume at the model core and its vertical displacement

The water volume in the model core changes dynamically as

$$\frac{d\text{Volume}_{\text{core}}(t)}{dt} = Q_{\text{in}}(t) - Q_{\text{out}}(t) \quad (12)$$

The water level in the model core, which is assumed responsible for some of the ground vertical movement, is proportional to

$$H_C(t) = \frac{\text{Volume}_{\text{core}}(t)}{A_{\text{core}}} \quad (13)$$

The equations delineate the mechanisms governing precipitation, percolation, and water flow within the considered CF area (Fig. 2b), which is made of two buffers at R_1 and R_2 characterized by different percolation speeds. This schematic model forms the basis for the subsequent numerical simulations.

5. Data analysis and empirical modeling

Fig. 7a and 7b depict the daily rainfall measurements across CF since 1970, and their cumulative totals for each 1-year period. The multi-year smooth red curve — obtained with the MATLAB function smooth, with Localized Scatterplot Smoothing (LOESS) = 0.2, which approximately corresponds to a moving average of 4 years — presented in Fig. 6b indicates a decline in annual rainfall from approximately 1300 mm/year in the 1970 s to 950 mm/year by around 1995. The rainfall decrease during this period was followed by an increase in rainfall between 1995 and 2010–2015, peaking at approximately 1250 mm/year, before stabilizing at an average of 1125 mm/year during the period spanning from 2019 to 2025. Furthermore, Fig. 7b illustrates interannual fluctuations characterized by recurring peaks, a climatic phenomenon commonly associated with the El Nino Southern Oscillation (ENSO) and the Northern Atlantic Oscillation (NAO) systems. Four of these prominent peaks (high amount events) are identified with red markers labeled A, B, C, and D.

Fig. 7c illustrates the vertical displacement recorded at the GNSS Rite Station. The rapid uplift observed during the 1984–1985 unrest, attributed to the uplift of Unit B shown in Fig. 4, was followed by a gradual subsidence totaling approximately 0.93 m, which persisted until 2004–2005. Subsequently, beginning in 2005, a monotonic and accelerating uplift is observed, which exceeded about 1.4 m in January 2025 (Bulletins of the OV-INGV, 2025). Fig. 7d presents the detrended vertical displacement, isolating its smooth component represented by the red curve in Fig. 7c. Fig. 7d identifies multiple interannual mini uplifts with an amplitude of about 4–5 cm. The four largest uplifts are denoted in the figure by letters A, B, C, and D (corresponding to the high rainfall events of Fig. 7b).

A visual comparative analysis of the graphs in Fig. 7 suggests a correlation between the multidecadal variations in annual rainfall (Fig. 7b) and the gradual vertical displacement observed at the GNSS Rite Station from 1985 to the present (Fig. 7c), with an approximate time-lag of 10–15 years from 1985 to about 1990–1995 and then increases until 2010–2015. Additionally, a comparison between the interannual fluctuations depicted in Fig. 7b and 7d shows a lagged correspondence, particularly for the four major peaks labeled with red letters A, B, C, and D in both graphs. This alignment occurs when accounting for a

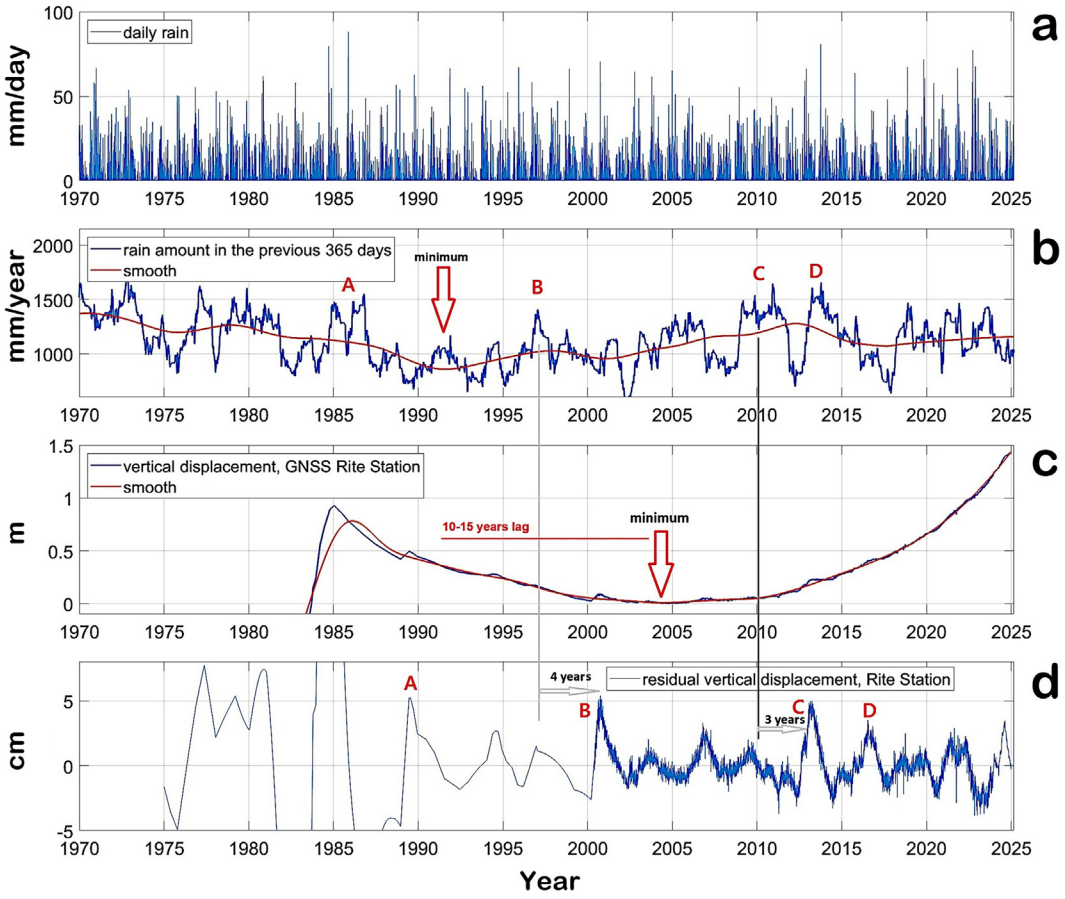

Fig. 7. (a) Daily rainfall measurements across Campi Flegrei since 1970. (b) Rainwater 1-year cumulative curve (blue line), with its multi-year smooth curve (red line); (c) Ground displacement (blue line) at the GNSS Rite Station with its multi-year smooth curve (red line). (d) Residual vertical displacement obtained by detrending the red curve from the blue curve in (c), which highlights several mini uplifts. The high rainfall events indicated by the points A, B, C and D in panel (b) are interpreted to have driven the significant mini-uplifts shown in panel (d) with time lags of about 4 years before 2005 and about 3 years after 2010.

time-lag of approximately 4 years for peaks A and B, and around 3 years for peaks C and D. This correspondence suggests that changes in rainfall patterns may have contributed to the ground vertical movement shown in Fig. 6c with time-lags of 4 and 3 years, respectively, because of the percolation times required by the meteoric water to reach the model core. After 2010 a 3-year time lag could indicate increased fracturing which facilitates rainwater percolation.

The graphs in Fig. 7d also show actual rainfall and vertical displacement data and the lagged correlation between rainfall patterns and CF ground uplift and multidecadal unrest is highlighted. Here, we propose an empirical model that aims to recreate this time lag between the rainfall record and the underground water accumulation function by simulating a simple hydrological flow model as described above.

The model incorporates several free parameters. The choice of the best approximate values of these parameters was done by a Monte Carlo method of running the model several times by changing the parameter values to obtain a good configuration that correlates the model outputs with the patterns of the vertical displacement at the GNSS Rite Station (Fig. 7c).

The main free parameters of the model were chosen as: R_0 = 1 km, R_1 = 3 km, and R_2 = 6 km, for the three concentric areas shown in Fig. 2b; h = 2 km depth; V_1 = 4 m/day (hydraulic conductivity) until 1996 and then it is assumed to gradually accelerate as a parabola to V_1 = 5 m/day in 2025; and $V_2 = \frac{2}{3}V_1$ because we assumed that the second buffer is less fractured than the first one (Fig. 2b).

The above hydraulic conductivity values are empirically assessed because the actual values in CF are unknown and, in any case, the actual hydraulic conductivity is highly variable because of the anisotropy of the permeability in CF area. In any case, a hydraulic conductivity of 4–5 m/day suggests that groundwater flows at an average speed of approximately 5×10^{-3} cm/s, or about 1.6 km/year. This flow rate is reasonable because it is typical in scenarios involving highly fractured igneous and metamorphic rocks, where hydraulic conductivity can reach values as high as 3×10^{-2} cm/s, corresponding to about 10 km/year (Freeze and Cherry, 1979). The model mean-field hydraulic conductivity from our model can be converted to an intrinsic permeability using the properties of the fluid. A hydraulic conductivity of 4 m/day is equivalent to an intrinsic mean-field medium permeability of 4×10^{-12} m^2 for an aqueous fluid (assumed pure H_2O) at 1 bar and 25 °C and 5.8×10^{-13} m^2 for an aqueous hydrothermal fluid at 700 bars (~3 km depth) and 350 °C. These estimated mean-field intrinsic permeabilities are consistent with weakly consolidated Quaternary marine and continental deposits and fractured volcanic and volcanoclastic lithologies in the shallow crustal section near Pozzuoli (Judenherc and Zollo, 2004; Milia and Torrente, 2020). The hydraulic conductivity V_1 is assumed to gradually accelerate from 4 to 5 m/day to reproduce the time lags of 4 and 3 years observed in Fig. 7d. The acceleration of the hydraulic conductivities (V_1 and V_2) could be explained by the observed increasing seismicity indicative of an enhanced local fracture permeability. High Gutenberg-Richter 'b' values of 1.3–1.7 in the earthquake swarm scaling relation $\log N = a - bM$ (N is the cumulative number of earthquakes with magnitude larger than M and a and b are constants) at depths less than 3 km is consistent with fracture-aided fluid migration in this region (Glazner and McNutt, 2021; Tramelli et al., 2024).

Fig. 8 shows the results obtained with the model described above under two drainage conditions (Model case #1 and Model case #2), as detailed below. The adopted two cases were useful because Eq. (1) has two different components (H_B and H_C), while the model is supposed to simulate only H_C. For this reason, we run the model for two extreme cases for the drainage timescale (τ), as detailed below.

Fig. 8 (left) shows the results obtained using Model case #1 that assumes that the drainage timescale is constant as $\tau(t) = 1$ year. Fig. 8 (right) shows the results obtained using Model case #2 that assumes that the drainage timescale is variable as: $\tau(t) = 1$ year until 1985 (just after the 1982–1984 unrest), then it decreases parabolically in time until $\tau(t) = 0.5$ year in t = 2007 (when the first mini uplift occurred after the beginning of the new uplift phase in year 2005) and finally to rise again parabolically until $\tau(t) = 1.5$ year in the year t = 2025 (Fig. 7c).

The drainage timescale, $\tau(t)$, represents the temporal scale over which underground water is discharged into the sea. A larger $\tau(t)$ corresponds to increased accumulation of water within Unit C. In Model case #1, when $\tau(t)$ is assumed to be constant, the estimated timescale is set to 1 year to approximately match the previously mean-field hydraulic conductivity of 1.6 km/year since Unit C is located about 1–2 km below the surface (Fig. 8a$_1$).

In Model case #2, $\tau(t)$ is assumed to change over time. During the subsidence period (1985–2005), $\tau(t)$ should have gradually decreased because the system opened to fluid circulation by fracture formation (Lima et al., 2025a and references therein). Conversely, during the uplift period (post-2007), $\tau(t)$ should have progressively increased as the uplift is a consequence of the closure of the system to fluid circulation (Fig. 8a$_2$).

The left and right panels of Fig. 8 show the results of the Model cases #1 and #2 run under the two discussed drainage scenarios: panels a$_1$ and a$_2$ report the model outputs given by Eq. (13) that provides the estimated underground water levels; panels b$_1$ and b$_2$ (which show the same graph for comparison) illustrate the vertical displacement recorded at the GNSS Rite Station; panels c$_1$ and c$_2$ show the residual of the model outputs detrended to remove the smooth component; and panels d$_1$ and d$_2$ (which show the same graph for comparison) show the residual of the vertical displacement shown in b$_1$ and b$_2$. The residual curves shown in Fig. 8 panels c$_1$ and c$_2$ reveal that the underground water rise function (Eq. (13)) exhibits interannual fluctuations that are strongly correlated with those observed in the vertical displacement recorded at the GNSS Rite Station. This relationship suggests that the observed mini uplifts (Fig. 3) may have been driven by variations resulting from fluctuations in underground water accumulation in Unit C (at approximately 1–2 km depth) beneath Pozzuoli.

The rainwater rise function (Fig. 8 panels c$_1$ and c$_2$) indicates that these water fluctuations have an amplitude of approximately 40–50 cm and are broadly consistent with the variations in vertical displacement recorded at the GNSS Rite Station (panel d), which have an amplitude of about 4–5 cm (Fig. 8 panels d$_1$ and d$_2$). This implies that to convert the vertical displacement with our empirically modelled water accumulation parameter H_C (Eq. (13)) we can use the conversion factor of roughly 10.

By using this empirical conversion factor also for the multidecadal scale, we now proceed to examine the implications arising from the two scenarios related to the drainage timescale $\tau(t)$.

The Model case #1 illustrated in Fig. 8a$_1$ indicates that the underground water level function, described by Eq. (13), increased by approximately 3 m from its minimum to its maximum. Using the conversion factor 10, 3 m corresponds to an estimated ~ 30 cm rise in the vertical displacement recorded at the GNSS Rite Station. Given that the total vertical displacement H_{B+C} from 2005 to January 2025 amounts to about 1.4 m, it can be inferred that $H_C \approx 0.3$ m and $H_B \approx 1.1$ m. Consequently, under the assumption that the drainage timescale remains constant over time, most of the uplift (~ 80%) observed at CF could be attributed to the uplift of deeper Unit B, located at a depth of approximately 3 km. In contrast, interannual changes to rainfall amount were responsible for

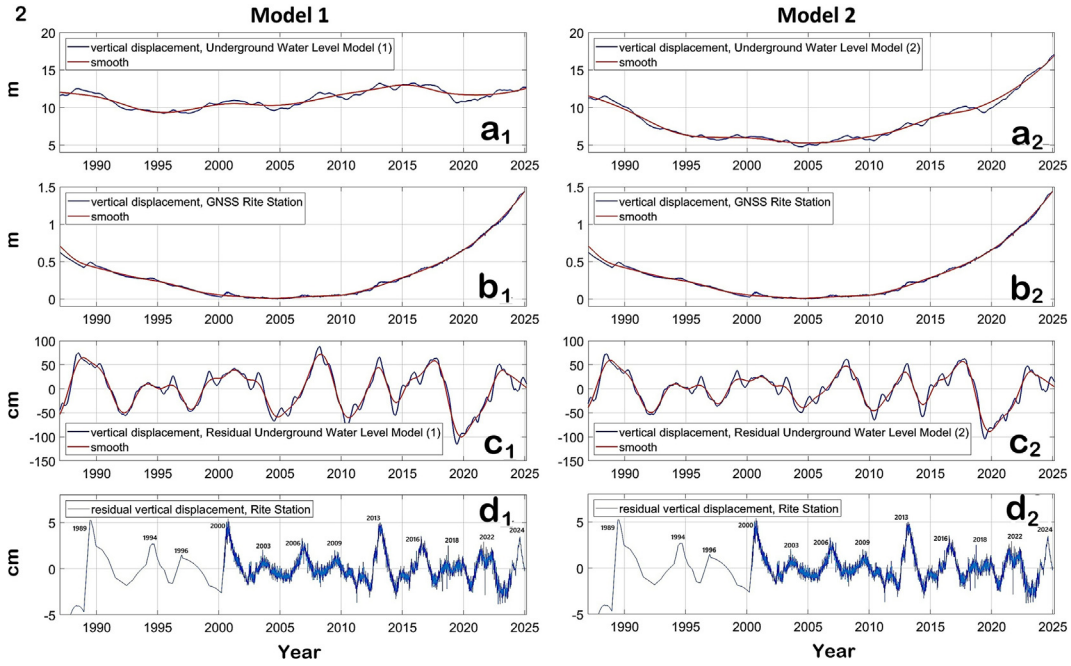

Fig. 8. Comparison between modelled groundwater accumulation and vertical ground movement as a function of the discharge time scale $\tau(t)$. (a_1) and (a_2) show the output of Eq. (13) in the model under the two conditions: (1) constant $\tau(t)$; (2) variable $\tau(t)$. (b_1) and (b_2), which are equal for comparison, show the ground displacement at the GNSS Rite Station; note the close multidecadal correlation between (a_2) and (b_2). (c_1) and (c_2) show the curves in (a_1) and (a_2) detrended of their interannual component after removing the smooth components. (d_1) and (d_2), which are equal for comparison, show the curves in (b_1) and (b_2) detrended of their interannual component after removing the smooth components.

the minor interannual uplifts, contributing roughly 20% to the total uplift from 2005 to 2025 by enlargement of Unit C, situated at adepth of about 1–2 km.

The statistical tests and their significance of the correlation between the modeled interannual groundwater accumulation fluctuations (blue curve in Fig. 8c_1) and the interannual variations in vertical displacement recorded at the GNSS Rite Station (Fig. 8d_1) are discussed in the Appendix. The Model case #2 presented in Fig. 8a_2 suggests that the underground water level function (Eq. (13)) increased by approximately 12 m from its 2005 minimum to its 2025 maximum. This rise corresponds to an estimated ~ 1. 2 m increase in the vertical displacement recorded at the GNSS Rite Station. Given that the total vertical displacement H_{B+C} from 2005 to January 2025 amounts to 1.4 m, it can be inferred that $H_C \approx 1.2$ m and $H_B \approx 0.2$ m. Under the assumption that the drainage timescale varied over time as hypothesized above, most of the uplift (~86%) observed at CF could be attributed to the enlargement of Unit C, situated at approximately 1–2 km depth meaning that the underground accumulation of meteoric water contributed to the interannual mini uplifts plus nearly 86% of the uplift from 2005 to 2025. Under this scenario, the contribution of Unit B to the overall uplift would be estimated as only ~14% of the total displacement.

It is, therefore, evident that the process is also highly sensitive to variations in the drainage timescale function $\tau(t)$. For instance, if $\tau(2025)$ is assumed to have risen to 1.7 years instead of the hypothesized 1.5 years, 100% of the total uplift would be attributed to underground water accumulation within Unit C. This extreme scenario may not be realistic since there is the need to explain why the drainage time scale should have increased during the last 20 years.

The two models indicate that fluctuations in precipitation over the past 40 years may have contributed to at least 20% of the total uplift (Model case #1) recorded at the GNSS Rite station between 2005 and 2025. However, considering the likelihood of a simultaneous increase in the drainage timescale (Model case #2) — potentially driven by heightened pressure beneath the closed Unit B — which could partially seal the drainage fractures, meteoric water may accumulate more and could have played a greater role in the total observed uplift. Thus, Unit B and Unit C may interact dynamically, as the uplift of Unit B could reduce drainage efficiency, leading to a longer timescale $\tau(t)$ and, therefore, to a major contribution of Unit C to the total uplift.

6. Discussion

The recent uplift of central Pozzuoli has been accompanied by shallower earthquake hypocenters compared to the 1982–1984 uplift episode (De Siena et al., 2017), indicating dynamic changes in the fractured system at depth. These changes are likely favored by additional rainwater infiltration into Unit C, which alters the hydrological loading rate and increases pore pressure, thereby enhancing seismicity. Elevated fluid pressure reduces the normal stress acting on fault planes and may exert a lubricating effect (e.g., Becken et al., 2011; Scuderi and Collettini, 2016, and references therein). Moreover, thermal expansion of pore fluids can further destabilize fault systems by decreasing effective stress across pre-existing zones of weakness, potentially triggering the numerous seismic swarms observed during the current phase of CF bradyseism (Guerriero and Mazzoli, 2021).

The schematic hydrodynamic circulation (Fig. 4) shows that it is strictly governed by the tectono-stratigraphic framework.

Subsequent meteoric fluid infiltration is linked to the ongoing stages of *syn*-folding fracturing. These folds are indicative of shallow-formed structures characterized by extensive networks of fractures and faults that enhance fluid mobility (Fig. 6c). This reconstruction has significant implications for understanding the dynamics of the area and forecasting future eruptions.

Based on the described stratigraphy, two main impermeable units define fluid-rich reservoirs located within Unit A and Unit C

(Fig. 4). The key impermeable layer is Unit B that covers the entire region. Seismic reflection profiles reveal that fluid accumulates within Unit A (Fig. 5b). Critically, above Unit B, the seismic horizons are parallel and continuous, demonstrating that Unit B effectively seals the underlying reservoir (Unit A). This confirms that sedimentary Unit B represents an impermeable barrier within the stratigraphic framework of Naples Bay and Campi Flegrei.

Further confirmation is provided by two distinct aquifers encountered in the Mofete 5 borehole. These findings support the existence of a regional impermeable layer. In this context, Unit A, located between the carbonate basement and Unit B, acts as a fluid-rich reservoir subject to overpressure conditions. Numerous earthquakes beneath Pozzuoli Bay occur within this unit.

The upper impermeable unit is the pyroclastic wedge, which partially seals the Unit C reservoir until it extends beneath the bay of Pozzuoli, where Reservoir C is not constrained and the fluids reach the surface forming undersea pockmarks (Figs. 4 and 5c). Beneath the Pozzuoli–Solfatara area, this boundary between Unit C and the impermeable pyroclastic unit lies between 0.5 and 1 km depth. Summarizing, a critical distinction emerges between the reservoirs of Unit A and Unit C. Unit A is uniformly sealed by Unit B across the basin, while Unit C is only sealed where the pyroclastic wedge is present and where bradyseism takes place. As illustrated in Fig. 4, in the absence of pyroclastic deposits above Unit C, fluids escape upward and discharge at the seafloor. This explains, along with the tectonic anticline formation under Pozzuoli Rite, why this area is affected by the maximum uplift.

Fig. 4 shows the reactivation of ancient normal faults during the deposition of pyroclastic wedges, particularly in the eastern part of the section. The tectonic event documented in Pozzuoli Bay over the last 8 ka (Milia and Torrente, 2000) corresponds to the formation of a *syn*-sedimentary fold, culminating in the Pozzuoli–Solfatara anticline — a highly faulted region where fault orientations follow regional tectonic trends (e.g., Bruno et al., 2007). In this context, tectonic inversion has folded the strata within zones bounded by reactivated normal faults.

The structural and stratigraphic permeability architecture critically influences fluid distribution and migration pathways (e.g., Sibson, 1996, 2003). These pathways generally involve downward percolation of meteoric and sea waters through fractures and upward movement of magmatic fluids. The depositional setting in which folds form governs a spectrum of fluid transport processes, with fluids driven from high- to low-pressure zones. Overall, deep hydrothermal systems are exceptionally water-rich, facilitating overpressure generation and fluid escape throughout the development of anticlines. This results in diverse fluid migration structures — from deep to shallow — such as mud dykes, sills, laccoliths, volcanoes, fluid escape pipes, crestal normal faults, and thrust faults. Among these, crestal anticline faults play a major role in transmitting fluids to upper fold regions (Evans and Fisher, 2012).

Within Unit C, upward fluid migration through folded strata is likely reflected by the seismicity occurring at depths of 1–2 km below the pyroclastic wedge (Unit D, Fig. 4). Faults beneath the crestal anticline — Solfatara, Pisciarelli, and Agnano — reach depths of around 2 km (Fig. 6c), enhancing the pyroclastic wedge's permeability and enabling fluid escape from Unit C.

These fluids rise through faults and mix locally with shallow groundwater (Aiuppa et al., 2006). Volcano-tectonic discontinuities in this zone also promote vertical mixing among meteoric water, deep CO_2-rich fluids, and seawater.

Once again, the "hydrothermal model" explains how Unit B (Fig. 4), which is subject to compressive tectonic stress due to the anticline formation, governs bradyseism over timescales from 1 to 100 years, acting as a valve between the hydrostatic and lithostatic systems. If fully sealed, Unit B could cause 40 m uplift (Lima et al., 2009). However, the fractured system prevents complete sealing, resulting in limited uplift or subsidence.

Connectivity between the two systems evolves cyclically through hydrothermal deposition of secondary minerals (reducing permeability) and fracture propagation (increasing permeability). This, along with the thermo-poroelastic properties of rocks (first advanced by Casertano et al., 1976), leads to alternating uplift and subsidence phases (Lima et al., 2025a, and references therein). Lima et al. (2025a) argue that in 2005, closure of fractures in Unit B and the increase in lithostatic pressure started both a new phase of ground uplift and a partial sealing of the fractures (by mineralization depositions, see: De Vivo et al., 1989; Belkin and De Vivo B., 2023; Belkin et al., 2023, 2024) and that the slower uplift velocity is due to the opening of new moderate fractures that allows the deep fluids to escape, reducing the pressure of magmatic fluid below the impermeable layer corresponding to Unit B (Fig. 4). These magmatic fluids would be released into the Reservoir C (Fig. 4b) as demonstrated by recent studies on the chemical-physical variations recorded in the Solfatara fumaroles (Calìro et al., 2025).

The present study complements previous research, taking into consideration the contribution of infiltrating meteoric water to the uplift of Pozzuoli Rite. The proposed model evaluates the infiltration of meteoric water under Pozzuoli and shows a correlation between the recharge of rainwater into the CF geothermal buffer and the uplift caused by the local bradyseism. Previous studies have identified correlations between rainfall events, tidal activity, and seismicity in the region (Palumbo, 1985; Mazzarella and Palumbo, 1989; Petrosino et al., 2018; Scafetta and Mazzarella, 2021) but not explicitly linked to the vertical ground movement. Those studies suggested triggering mechanisms due to meteoric and sea water infiltration as well as lunar and solar tidal effects. For instance, on March 13, 2025, the most significant seismic event in the past 40 years (M = 4.6, made up of two close earthquakes) coincided with a full Moon, several days of low atmospheric pressure in the Campanian Plain, and heavy rainfall. Rainfall, low atmospheric pressure, and tidal activity act as perturbing factors in a critically balanced system.

Petrosino et al. (2018) and Scafetta and Mazzarella (2021) observed that rainfall does not always trigger earthquakes at CF, nor are all seismic events necessarily caused by water infiltration. In fact, CF area is inherently seismically active due to bradyseism dynamics caused mostly by magmatic fluids being continuously released from the crystallizing magma (>7.5 km deep), with its crystallization front migrating downward (Fig. 4; Burnham, 1979).

Such magmatic fluids, at lithostatic pressure, are trapped at depth by the impermeable Unit B (Fig. 4), until the effective stress exceeds the fracture strength, creating low magnitude seismic events, and the transfer of fluids into Unit C.

The novelty of our study lies in analyzing long-term rainfall data (from 1950) using a simple hydrogeological model (section 5) to assess variations of meteoric water underground infiltration since at least 1985 correlated with the detailed tectonic stratigraphic reconstruction of CF volcanic system. The hypothesis of the model is that the CF system can be subdivided into three concentric areas with a central reservoir below Pozzuoli Rite that can accumulate infiltrated meteoric water because it has an anticline structure with two reservoirs constrained between two impermeable layers (Figs. 4 and 6), which do not allow the fluid to easily discharge causing an overpressure. For lack of data, only empirically average hydraulic conductivities for each area are considered. The estimated hydraulic conductivities, when converted to intrinsic permeability, are reasonably consistent with lithologies like those of CF area.

Morphologically, the CF region near Astroni-Solfatara is a seismically active highly fractured zone that serves as an efficient col-

lector of meteoric waters (Figs. 4 and 6c). In particular, the Astroni crater is an area covering ~ 2.5 × 10^6 m^2 upstream Solfatara-Pisciarelli area (Fig. 2b), which contains a small lake of ~ 5 × 10^4 m^2 at its bottom. Another significant basin east of Solfatara is the Agnano crater (~3 × 10^6 m^2), which hosted a volcanic lake (~10^6 m^2) until it was drained via channels constructed in 1870. Additional craters, like Lake Avernus (Fig. 2b), are also found on the western side of Pozzuoli. Fig. 7b shows that the 365-day meteoric water amount function in the CF area presents interannual peaks every few years (which are indicated with the letters A, B, C, D). Fig. 7d shows, instead, the residual curve of the vertical displacement in Pozzuoli Rite Station (Fig. 7c). By comparing Fig. 7b and 7d, it is observed that the meteoric water amount function correlates well with the function describing the vertical displacement of the Pozzuoli area both at the decadal and interannual scales. In fact, rainfall amount decreased from the late 1970 s to about 1990–1995 and then increases until 2010–2015 and remained approximately constant until date (Fig. 7b). This pattern correlates well, with a time lag of 10–15 years with the vertical displacement decrease from 1985 to 2005 and the subsequent uplift until the present (Fig. 7c). Instead, the time-lag between the interannual mini-uplift peaks of rainwater amount is about 4 years prior to 2010 (Fig. 7d), then it decreases to about 3 years afterward, indicating an increase in hydraulic conductivity.

The proposed model was used to simulate if the infiltration of meteoric water in the reservoir of Unit C under Pozzuoli Rite can contribute to the observed uplift dynamics. To explain the observed lagged correlations shown in Fig. 7, we take into consideration that the rainwater accumulation also depends on a timescale $\tau(t)$ of discharge that could change in time because of the seismicity of the area. The model simulations are shown in Fig. 8. Here, we model two different cases: Model #1 uses a constant timescale $\tau(t)$ of discharge; Model #2 uses a variable timescale $\tau(t)$ of discharge. The increase in the timescale $\tau(t)$ of the drainage in Model #2 (Fig. 8 right) leads to an increase in the contribution of rainwater penetrating in Unit C to the total uplift.

The model simulations suggest that the interannual mini uplifts are related to the interannual variation of rainfall amount. For example, the strong mini uplift that occurred in 1989 (point A in Fig. 7d) could have been triggered by the significant increase in rainwater between 1985 and 1987 (point A in Fig. 7b). The same lagged correlation of about 3–4 years between interannual rainwater maxima and all observed mini uplifts of about 4–5 cm is evident by comparing Fig. 7b and 7d, and the water processed signals in Fig. 8c_1 and 8c_2.

In fact, both Model cases #1 and #2 show that the interannual variations of the meteoric water infiltration within Unit C correlate well with all observed mini uplifts (Fig. 8c and 8d). The time-lag observed with the rainwater amount is covered by the percolation times that the meteoric water, falling on the land of CF area, needs to reach the model core under Pozzuoli Rite (Fig. 4, area "Eb"). In summary, the results of this study (Fig. 8) indicate that an increase in rainwater infiltration has occurred from 2004 to 2005, likely along with Unit B sealing and the beginning of a new phase of ground uplift. We interpret that the total uplift is the combined contribution of both the fluid pressure, mostly of magmatic origin under the impermeable Unit B, and of meteoric water penetrating in Unit C under the impermeable pyroclastic Unit. Our Model #1 suggests that meteoric water accumulation under Pozzuoli Rite has contributed a minimum of 20% of the total uplift (Fig. 8a_1). Model 2, instead, implies a larger contribution to the total uplift of meteoric water accumulation in Unit C because it supposes that Unit B can control the fracturing of the system that can change the drainage timescale $\tau(t)$. In the present case, it is likely that $\tau(t)$ has increased since 2005 (Fig. 7c) when the uplift slowly started.

A final consideration is that tectonic events on a regional scale could have an impact on bradyseism. For example, the rapid uplift recorded between 1982 and 1984, when approximately 1.80 m of ground inflation occurred in just two years, could have been a consequence of the 1980 Irpinia earthquake of *M* 6.9 (Bernard and Zollo, 1989), located about 90 km from CF. It could be hypothesized that the latter triggered — within two years — fracturing of the crystallized carapace of the deep magma chamber with the release of magmatic fluids in Reservoir A (Fig. 4) causing an increase of lithostatic pressure acting as a powerful driver of unrest. Even the eruption of Vesuvius in 79 AD is thought to have been triggered — after a long repose time — by a regional earthquake that struck 15 years earlier (Morgan et al., 2006).

7. Conclusions

This study documents the contributions of fluids having diverse origins to drive ground deformation and seismic activity in the geologically and tectonically complex CF area of southern Italy. Specifically, this work suggests a direct dynamic link between multiscale temporal rainfall patterns and bradyseism in CF, Italy. This connection necessarily involves time-lags, as rainwater must percolate through subsurface layers to reach the accumulation core located beneath Pozzuoli, at approximately 1–2 km depth. This temporal delay has been hydrologically modeled and is consistent with the hydrogeologic properties of the sediments and lithologies underlying the region.

The observed shift in time lags — from about 4 years before 2010 to roughly 3 years afterward — between interannual fluctuations (mini uplifts of 4–5 cm), may indicate that the hydraulic conductivity slightly increased from 2005 to date, possibly resulting from enhanced intrinsic permeability due to increased fracturing caused by seismic activity associated with the accelerated uplift rate since 2010.

The multidecadal pattern of ground deformation, characterized by subsidence from 1985 to 2005 followed by uplift since 2005, appears correlated with a similar variation in the rainfall record, with an estimated lag of around 10–15 years. The hydrological Model #1 estimates that about 20% of the 1.4 m uplift since 2005 may be attributed to groundwater infiltration. However, this percentage could increase depending on the drainage efficiency determined by a variable timescale $\tau(t)$ of discharge, as demonstrated by Model #2.

The proposed model underscores the significant role of rainfall input in the current unrest and offers a quantitative framework for estimating its contribution. To mitigate uplifts and to keep constant the underground meteoric water level in Unit C below Pozzuoli we estimated that it is necessary to draw something of the order of 1000 m^3 of underground water per hour.

Our results suggest also that a strategic mitigation measure could be to drain the surface meteoric water at the CF area and, particularly, that falling inside the Astroni crater located upstream from Solfatara–Pisciarelli. Historically, such an intervention would resemble the project carried out in the Agnano crater in 1870, when surface water accumulation formed a lake. Today, the Solfatara–Pisciarelli remains the most concerning area for public safety. However, the main benefits of such intervention may become relevant only after a few years, due to the time required by the meteoric water to percolate into Unit C below Pozzuoli. In any case, meteoric water may trigger the local seismic activity within few days or weeks from rain events because infiltration of rainwater could lubricate superficial faults (Scafetta and Mazzarella, 2021).

Fracturing at the apex of the anticline beneath the Solfatara crater is particularly intense, forming a network of fractures that terminate at approximately 2 km depth, resulting in shallow seismic

activity. Conversely, in the Bay of Pozzuoli, fracturing at the syncline extends to greater depths, which gives rise to deeper seismicity. Additionally, earthquakes with magnitudes equal to or greater than 4 are concentrated along the main faults affecting the area and witness the reactivation of the preexisting faults during the present tectonic activity. Finally, the tectono-stratigraphic architecture of the CF area raises questions about the interpretation of the CF volcanic system as a caldera.

CRediT authorship contribution statement

Nicola Scafetta: Writing – review & editing, Writing – original draft, Visualization, Validation, Software, Methodology, Investigation, Formal analysis, Data curation, Conceptualization. **Annamaria Lima:** Writing – review & editing, Writing – original draft, Supervision, Investigation. **Alfonsa Milia:** Writing – review & editing, Writing – original draft, Visualization, Investigation, Data curation, Conceptualization. **Frank Spera:** Writing – review & editing. **Robert J. Bodnar:** Writing – review & editing. **Benedetto De Vivo:** Writing – review & editing. **Linda Daniele:** Writing – review & editing.

Declaration of competing interest

The authors declare that they have no known competing financial interests or personal relationships that could have appeared to influence the work reported in this paper. Corresponding author Nicola Scafetta is an Associate Editor of this Journal and was not involved in the editorial review or the decision to publish this article.

Appendix:. Statistical test

To test the statistical significance of the observed correlation between the interannual water accumulation fluctuations (blue curve in Fig. 8c_1) and the interannual variations in vertical displacement recorded at the GNSS Rite Station (Fig. 8d_1) we adopt three methodologies:

(1) The direct Pearson linear correlation between the two curves depicted in Fig. 8c_1 and 8d_1 gives a correlation coefficient R_o = 0.127 that, for the 13,879 daily data from 01/01/1987 to 12/30/2024, gives a confidence probability of $P \ll 0.000001$, which means that the two curves are highly correlated.

(2) We use a Monte Carlo approach to test whether random rainfall records with mean and standard deviation equal to the real one could produce water accumulation curves with correlation results statistically compatible with that obtained using the real data, R_o = 0.127, which is assessed above in point 1. To accomplish this, we shuffle the original daily rain record to reproduce 1000 synthetic daily rain records with the same length of the original one. The random shuffling destroys the autocorrelation patterns observed in the data but conserves its mean and standard deviation of the record. Thus, the test can assess the correlation relevance of the specific dynamics present in the rainfall record, as processed by Model 1, with the interannual variations in vertical displacement recorded at the GNSS Rite Station (Fig. 8d_1). Each of the produced 1000 synthetic daily rain amount records are processed by Model 1 to produce 1000 synthetic interannual water accumulation fluctuations equivalent to those shown by the blue curve in Fig. 8c_1. We evaluate the Pearson linear correlation coefficients, R_i (i = 1,. . ., 1000), between these 1000 synthetic records with the interannual variations in vertical displacement recorded at the GNSS Rite Station (Fig. 8d_1) from 01/01/1987 to 12/30/2024. We found that 81% of the 1000 synthetic records produced R values lower than R_o, which is the correlation coefficient found above in point 1. Moreover, we calculate the standard deviation, A_i (i = 1,. . ., 1000), of these 1000 synthetic records from 01/01/1987 to 12/30/2024 as estimates the amplitude of the produced fluctuations. We calculate the standard deviation of the real interannual water accumulation fluctuation record to be A_o = 42 cm. We found that the distribution of the 1000 A_i (i = 1,. . ., 1000), of the synthetic records has an average μ = 26 cm and a standard deviation σ = 5 cm. This means that the real A_o = 42 cm is outside the typical three-sigma range of the synthetic ensemble which covers around 99.7% of the total probability; therefore, from a statistical point of view the ensemble of the 1000 synthetic water accumulation records is not statistically compatible with the actual one.

(3) If instead of the rain record, it is shuffled the interannual variations in vertical displacement recorded at the GNSS Rite Station (Fig. 8d_1), we found that 100% of the 1000 synthetic records produced R values lower than Ro.

The above tests suggest that the interannual water accumulation fluctuation record obtained with actual data shows dynamical patterns much more pronounced than those obtained with the synthetic ones, and these patterns appear to be sufficiently well correlated with the interannual variations in vertical displacement recorded at the GNSS Rite Station (Fig. 8d_1) as suggested by the statistical test in point 1.

References

AGIP, 1987. Geologia e geofisica del sistema geotermico dei Campi Flegrei. Internal report, AGIP S.p.A., Milan, Italy (in Italian).

Aiuppa, A., Federico, C., Giudice, G., Gurrieri, S., Liuzzo, M., Shinohara, H., Favara, R., Valenza, M., 2006. Rates of carbon dioxide plume degassing from Mount Etna volcano. J. Geophys. Res. Solid Earth 111, B09207. https://doi.org/10.1029/2006JB004307.

Bear, J., 1972. Dynamics of Fluids in Porous Media. Reprinted by Dover Publications, Elsevier, New York, p. 1988.

Becken, M., Ritter, O., Bedrosian, P.A., Weckmann, U., 2011. Correlation between deep fluids, tremor and creep along the central San Andreas fault. Nature 480 (7375), 87–90. https://doi.org/10.1038/nature10609.

Belkin, H.E., De Vivo, B., 2023. Compositional variation and zoning of epidote supergroup minerals in the Campi Flegrei geothermal field, Naples, Italy. Eur. J. Mineral. 35, 25–44. https://doi.org/10.5194/ejm-35-25-2023.

Belkin, H.E., McAleer, R.J., De Vivo, B., Croke, M.R., 2023. Mofete and San Vito geothermal field ore mineralization data [dataset]. U.S. Geological Survey Data Release. https://doi.org/10.5066/P9HNDG4F.

Belkin, H.E., McAleer, R.J., De Vivo, B., 2024. Ore mineralization in the Mofete and San Vito geothermal fields, Campi Flegrei volcanic complex, Naples, Italy. J. Geochem. Explor. 264, 107556. https://doi.org/10.1016/j.gexplo.2024.107556.

Bernard, P., Zollo, A., 1989. The Irpinia (Italy) 1980 earthquake: Detailed analysis of a complex normal faulting. J. Geophys. Res. Solid Earth 94 (B2), 1631–1647. https://doi.org/10.1029/JB094iB02p01631.

Bernasconi, A., Bruni, P., Gorla, L., Principe, C., Sbrana, A., 1981. Risultati preliminari dell'esplorazione geotermica profonda nell'area vulcanica del Somma-Vesuvio. Rend. Soc. Geol. Ital. 4, 237–240 (in Italian).

Bevilacqua, A., Neri, A., De Martino, P., Giudicepietro, F., Macedonio, G., Ricciolino, P., 2024. Simulation of eruption scenarios and hazard quantification at Campi Flegrei caldera. Commun. Earth Environ. 5, 742. https://doi.org/10.1038/s43247-024-01865-y.

Bodnar, R.J., Cannatelli, C., De Vivo, B., Lima, A., Belkin, H.E., Milia, A., 2007. Quantitative model for magma degassing and ground deformation (bradyseism) at Campi Flegrei, Italy: Implications for future eruptions. Geology 35 (9), 791–794. https://doi.org/10.1130/G23653A.1.

Bonafede, M., Mazzanti, M., 1997. Hot fluid migration in compressible saturated porous media. Geophys. J. Int. 128, 383–398. https://doi.org/10.1111/j.1365-246X.1997.tb01562.x.

Brocchini, D., Principe, C., Castradori, D., Laurenzi, M.A., Gorla, L., 2001. Quaternary evolution of the southern sector of the Campanian Plain and early Somma–Vesuvius activity: Insights from the Trecase 1 well. Mineral. Petrol. 73 (1–2), 67–91. https://doi.org/10.1007/s007100170011.

Bruno, P.G., Ricciardi, G.P., Petrillo, Z., Di Fiore, V., Troiano, A., Chiodini, G., 2007. Geophysical and hydrogeological experiments from a shallow hydrothermal system at Solfatara Volcano, Campi Flegrei, Italy: Response to caldera unrest. J. Geophys. Res. Solid Earth 112, B06201. https://doi.org/10.1029/2006JB004383.

Burnham, C.W., 1979. Magmas and hydrothermal fluids. In: Barnes, H.L. (Ed.), Geochemistry of Hydrothermal Ore Deposits. Wiley, New York, pp. 71–136.

Calìro, S., Avino, R., Capecchiacci, F., Carandente, A., Chiodini, G., Cuoco, E., Minopoli, C., Rufino, F., Santi, A., Rizzo, A.L., Aiuppa, A., Allocca, V., De Vita, P., Di Vito, M.A., 2025. Chemical and isotopic characterization of groundwater and thermal waters from the Campi Flegrei caldera (southern Italy). J. Volcanol. Geotherm. Res. 460, 108280. https://doi.org/10.1016/j.jvolgeores.2025.108280.

Cannatelli, C., Spera, F.J., Bodnar, R.J., Lima, A., De Vivo, B., 2020. Ground movement (bradyseism) in the Campi Flegrei volcanic area: A review. In: De Vivo, B., Belkin, H.E., Rolandi, G. (Eds.), Vesuvius, Campi Flegrei, and Campanian Volcanism. Elsevier, Amsterdam, pp. 407–433.

Caprarelli, G., Tsutsumi, M., Turi, B., 1997. Chemical and isotopic signatures of the basement rocks from the Campi Flegrei geothermal field (Naples, southern Italy): Inferences about the origin and evolution of its hydrothermal fluids. J. Volcanol. Geotherm. Res. 76, 63–82. https://doi.org/10.1016/S0377-0273(96)00072-8.

Carella, R., Guglielminetti, M., 1983. In: Buffers in the Mofete Field, Naples, Italy, In: Proceedings of the 9th Workshop on Geothermal Reservoir Engineering. Stanford University, Stanford, CA.

Carlino, S., 2021. Brief history of volcanic risk in the Neapolitan area (Campania, Southern Italy): A critical review. Nat. Hazards Earth Syst. Sci. 21, 3097–3112. https://doi.org/10.5194/nhess-21-3097-2021.

Casertano, L., Oliveri del Castillo, A., Quagliariello, M.T., 1976. Hydrodynamics and geodynamics in the Phlegrean Fields area of Italy. Nature 264, 154–161. https://doi.org/10.1038/264161a0.

Cerrone, C., Ascione, A., Robustelli, G., Tuccimei, P., Soligo, M., Balassone, G., Mormone, A., 2021. Late Quaternary uplift and sea level fluctuations along the Tyrrhenian margin of Basilicata–northern Calabria (southern Italy): New constraints from raised paleoshorelines. Geomorphology 395, 107978. https://doi.org/10.1016/j.geomorph.2021.107978.

Chiodini, G., Giudicepietro, F., Vandemeulebrouck, J., Aiuppa, A., Caliro, S., De Cesare, W., Tamburello, G., Avino, R., Orazi, M., D'Auria, L., 2017. Fumarolic tremor and geochemical signals during a volcanic unrest. Geology 45 (12), 1131–1134. https://doi.org/10.1130/G39447.1.

Cipriani, A., Marianelli, P., Sbrana, A., 2008. Studio di una sequenza piroclastica del vulcano della Solfatara (Campi Flegrei). Considerazioni vulcanologiche e sul sistema di alimentazione. Boll. Soc. Tosc. Sci. Nat. Ser. A 113, 39–48 (in Italian).

De Landro, G., Vanorio, T., Muzellec, T., Russo, G., Lomax, A., Virieux, J., Zollo, A., 2025. 3D structure and dynamics of Campi Flegrei enhance multi-hazard assessment. Nat. Commun. 16, 59821. https://doi.org/10.1038/s41467-025-59821-z.

Del Gaudio, C., Aquino, I., Ricciardi, G.P., Ricco, C., Scandone, R., 2010. Unrest episodes at Campi Flegrei: A reconstruction of vertical ground movements during 1905–2009. J. Volcanol. Geotherm. Res. 195 (1), 48–56. https://doi.org/10.1016/j.jvolgeores.2010.05.014.

De Siena, L., Chiodini, G., Vilardo, G., Del Pezzo, E., Castellano, M., Colombelli, S., Tisato, N., Ventura, G., 2017. Source and dynamics of a volcanic caldera unrest: Campi Flegrei, 1983–84. Sci. Rep. 7, 8099. https://doi.org/10.1038/s41598-017-08192-7.

Detournay, E., Cheng, A.H.D., 1993. Fundamentals of poroelasticity. In: Fairhurst, C. (Ed.), Comprehensive Rock Engineering: Principles, Practice and Projects, Vol. II. Pergamon Press, Oxford, pp. 113–171.

De Vivo, B., Belkin, H.E., Barbieri, M., Chelini, W., Lattanzi, P., Lima, A., Tolomeo, L., 1989. The Campi Flegrei (Italy) geothermal system: A fluid inclusion study of the Mofete and San Vito fields. J. Volcanol. Geotherm. Res. 36 (4), 303–326. https://doi.org/10.1016/0377-0273(89)90076-0.

De Vivo, B., Rolandi, G., Gans, P.B., Calvert, A., Bohrson, W.A., Spera, F.J., Belkin, H.E., 2001. New constraints on the pyroclastic eruptive history of the Campanian volcanic Plain (Italy). Mineral. Petrol. 73, 47–65. https://doi.org/10.1007/s007100170010.

De Vivo, B., Lima, A., 2006. A hydrothermal model for ground movements (bradyseism) at Campi Flegrei, Italy. In: De Vivo, B. (Ed.), Volcanism in the Campania Plain: Vesuvius, Campi Flegrei and Ignimbrites. Dev. Volcanol. 9. Elsevier, Amsterdam, pp. 289–317.

De Vivo, B., Lima, A., Bodnar, R.J., Milia, A., Spera, F.J., 2009. Il rischio di eruzione nei Campi Flegrei. Le Scienze 496, 96–103 (in Italian).

De Vivo, B., Rolandi, G., 2020. Volcanological risk associated with Vesuvius and Campi Flegrei. In: De Vivo, B., Belkin, H.E., Rolandi, G. (Eds.), Vesuvius, Campi Flegrei, and Campanian Volcanism. Elsevier, Amsterdam, pp. 471–492.

Evans, M.A., Fisher, M.P., 2012. On the distribution of fluids in folds: A review of controlling factors and processes. J. Struct. Geol. 44, 2–24. https://doi.org/10.1016/j.jsg.2012.08.003.

Farquharson, J.I., Amelung, F., 2020. Extreme rainfall triggered the 2018 rift eruption at Kīlauea Volcano. Nature 580, 491–495. https://doi.org/10.1038/s41586-020-2172-5.

Fortelli, A., Scafetta, N., Mazzarella, A., 2019. Nowcasting and real-time monitoring of heavy rainfall events inducing flash-floods: An application to Phlegraean area (Central-Southern Italy). Nat. Hazards 97, 861–889. https://doi.org/10.1007/s11069-019-03680-7.

Freeze, R.A., Cherry, J.A., 1979. Groundwater. Prentice-Hall Inc., Englewood Cliffs, NJ.

Glazner, A.F., McNutt, S.R., 2021. Relationship between dike injection and b-value for volcanic earthquake swarms. J. Geophys. Res. Solid Earth 126, e2020JB021631. https://doi.org/10.1029/2020JB021631.

Guerriero, V., Mazzoli, S., 2021. Theory of effective stress in soil and rock and implications for fracturing processes: A review. Geosciences 11 (3), 119. https://doi.org/10.3390/geosciences11030119.

Hainzl, S., Kraft, T., Wassermann, J., Igel, H., Schmedes, E., 2006. Evidence for rainfall-triggered earthquake activity. Geophys. Res. Lett. 33 (19), L19303. https://doi.org/10.1029/2006GL027642.

Hersbach, H., Bell, B., Berrisford, P., 2020. The ERA5 global reanalysis. Q. J. R. Meteorol. Soc. 146 (730), 1999–2049. https://doi.org/10.1002/qj.3803.

Husen, S., Bachmann, C., Giardini, D., 2007. Locally triggered seismicity in the central Swiss Alps following the large rainfall event of August 2005. Geophys. J. Int. 171 (3), 1126–1134. https://doi.org/10.1111/j.1365-246X.2007.03561.x.

Isaia, R., Troiano, A., Di Giuseppe, M.G., De Paola, C., Gottsmann, J., Pagliara, F., Smith, V.C., Stock, M.J., 2025. 3D magnetotelluric imaging of a transcrustal magma system beneath the Campi Flegrei caldera, southern Italy. Commun. Earth Environ. 6, 213. https://doi.org/10.1038/s43247-025-02185-5.

Jiménez, M.J., García-Fernández, M., 2000. Occurrence of shallow earthquakes following periods of intense rainfall in Tenerife, Canary Islands. J. Volcanol. Geotherm. Res. 103 (1–4), 463–468. https://doi.org/10.1016/S0377-0273(00)00237-7.

Judenherc, S., Zollo, A., 2004. The bay of Naples (Southern Italy): Constraints on the volcanic structures inferred from a dense seismic survey. J. Geophys. Res. Solid Earth 109, B10312. https://doi.org/10.1029/2003JB002876.

Kraft, T., Wassermann, J., Schmedes, E., Igel, H., 2006. Meteorological triggering of earthquake swarms at Mt. Hochstaufen, SE-Germany. Tectonophysics 424 (3–4), 245–258. https://doi.org/10.1016/j.tecto.2006.03.044.

Lima, A., De Vivo, B., Spera, F.J., Bodnar, R.J., Milia, A., Nunziata, C., Belkin, H.E., Cannatelli, C., 2009. Thermodynamic model for the uplift and deflation episodes (bradyseism) associated with magmatic–hydrothermal activity at the Campi Flegrei active volcanic center (Italy). Earth-Sci. Rev. 97, 44–58. https://doi.org/10.1016/j.earscirev.2009.10.001.

Lima, A., Bodnar, R.J., De Vivo, B., Spera, F.J., Belkin, H.E., 2021. Interpretation of recent unrest events (bradyseism) at Campi Flegrei, Napoli (Italy): Comparison of models based on cyclical hydrothermal events versus shallow magmatic intrusive events. Geofluids 2021, 2000255. https://doi.org/10.1155/2021/2000255.

Lima, A., Bodnar, R.J., De Vivo, B., Spera, F.J., Belkin, H.E., 2025a. The "breathing" Earth (la terra che respira) at Solfatara–Pisciarelli (Campi Flegrei, southern Italy) during 2005–2024: Nature's way of attenuating the effects of bradyseism through gradual and episodic release of subsurface pressure. Am. Mineral. 110, 820–825. https://doi.org/10.2138/am-2024-9516.

Lima, A., Macedonio, G., Esposito, R., Belkin, H.E., 2025b. Magma–carbonate country rock interaction can provide HO during magma ascent: Results from fluid and melt inclusions in skarn xenoliths from Breccia Museo, Campi Flegrei (Southern Italy). J. Volcanol. Geotherm. Res. 466, 108405. https://doi.org/10.1016/j.jvolgeores.2025.108405.

Mantiloni, L., Hickey, J., Alshembari, R., 2025. The role of gravity in the state of stress and pore pressure of poroelastic rocks. Geophys. J. Int. 242 (1), ggaf169. https://doi.org/10.1093/gji/ggaf169.

Marini, L., Principe, C., Lelli, M., 2022. The Solfatara Magmatic–Hydrothermal System: Geochemistry, Geothermometry and Geobarometry of Fumarolic Fluids. Advances in Volcanology. Springer, Cham, 375 pp. https://doi.org/10.1007/978-3-030-98471-7.

Marini, L., Principe, C., Lelli, M., 2025. Time changes during the last 40 years in the Solfatara magmatic–hydrothermal system (Campi Flegrei, Italy): New conceptual model and future scenarios. Solid Earth 16, 551–578. https://doi.org/10.5194/se-16-551-2025.

Mastin, L.G., 1993. Can Rain Cause Volcanic Eruptions? U.S. Geological Survey Open-File Report, 93–445.

Mazzarella, A., Palumbo, A., 1989. Does the solar cycle modulate seismic and volcanic activity? J. Volcanol. Geotherm. Res. 39, 89–93. https://doi.org/10.1016/0377-0273(89)90023-1.

Milia, A., Torrente, M.M., 1997. Evoluzione tettonica della Penisola Sorrentina (margine peritirrenico campano). Boll. Soc. Geol. Ital. 116, 487–502 (in Italian).

Milia, A., Torrente, M.M., 1999. Tectonics and stratigraphic architecture of a peri-Tyrrhenian half-graben (Bay of Naples, Italy). Tectonophysics 315, 301–318. https://doi.org/10.1016/S0040-1951(99)00280-2.

Milia, A., 2000. The Dohrn Canyon formation: A response to the eustatic fall and tectonic uplift of the outer shelf (Eastern Tyrrhenian Sea margin, Italy). Geo-Mar. Lett. 20, 101–108.

Milia, A., Torrente, M.M., 2000. Fold uplift and synkinematic stratal architectures in a region of active transtensional tectonics and volcanism, eastern Tyrrhenian Sea. Geol. Soc. Am. Bull. 112 (10), 1531–1542. https://doi.org/10.1130/0016-7606(2000)112.1531:FUASSA>2.0.CO;2.

Milia, A., Torrente, M.M., Giordano, F., 2000. Active deformation and volcanism offshore Campi Flegrei, Italy: New data from high-resolution seismic reflection profiles. Mar. Geol. 171 (1–4), 61–73. https://doi.org/10.1016/S0025-3227(00)00111-0.

Milia, A., Giordano, F., 2002. Holocene stratigraphy and depositional architecture of eastern Pozzuoli Bay (eastern Tyrrhenian Sea margin, Italy): The influence of tectonics and wave-induced currents. Geo-Mar. Lett. 22, 42–50. https://doi.org/10.1007/s00367-002-0095-9.

Milia, A., Torrente, M.M., 2003. Late Quaternary volcanism and transtensional tectonics in the Bay of Naples, Campania continental margin, Italy. Mineral. Petrol. 79 (1–2), 49–65.
Milia, A., Torrente, M.M., Russo, M., Zuppetta, A., 2003. Tectonics and crustal structure of the Campania continental margin: Relationships with volcanism. Mineral. Petrol. 79, 33–47. https://doi.org/10.1007/s00710-003-0005-5.
Milia, A., Torrente, M.M., Giordano, F., Mirabile, L., 2006. Rapid changes of the accommodation space in the Late Quaternary succession of Naples Bay, Italy: The influence of volcanism and tectonics. In: De Vivo, B. (Ed.), Volcanism of the Campania Plain. Dev. Volcanol. 9. Elsevier, Amsterdam, pp. 53–68.
Milia, A., Torrente, M.M., 2011. The possible role of extensional faults in localizing magmatic activity: A crustal model for the Campanian Volcanic Zone (eastern Tyrrhenian Sea, Italy). J. Geol. Soc. 168, 471–484. https://doi.org/10.1144/0016-76492010-121.
Milia, A., Torrente, M.M., 2015a. Tectono-stratigraphic signature of a rapid multistage subsiding rift basin in the Tyrrhenian–Apennine hinge zone (Italy): A possible interaction of upper plate with subducting slab. J. Geodyn. 86, 42–60. https://doi.org/10.1016/j.jog.2015.02.005.
Milia, A., Torrente, M.M., 2015b. Rift and supradetachment basins during extension: Insight from the Tyrrhenian rift. J. Geol. Soc. 172 (1), 5–8. https://doi.org/10.1144/jgs2014-046.
Milia, A., Torrente, M.M., 2020. Space–time evolution of an active volcanic field in an extensional region: The example of the Campania margin (eastern Tyrrhenian Sea). In: De Vivo, B., Belkin, H.E., Rolandi, G. (Eds.), Vesuvius, Campi Flegrei, and Campanian Volcanism. Elsevier, Amsterdam, pp. 297–321.
Montgomery-Brown, E.K., Shelly, D.R., Hsieh, P.A., 2019. Snowmelt-triggered earthquake swarms at the margin of Long Valley Caldera, California. Geophys. Res. Lett. 46 (7), 3698–3705. https://doi.org/10.1029/2019GL082254.
Morgan, D.J., Blake, S., Rogers, N.W., De Vivo, B., Rolandi, G., Davidson, J.P., 2006. Magma chamber recharge at Vesuvius in the century prior to the eruption of A. D. 79. Geology 34 (10), 845–848. https://doi.org/10.1130/G22604.1.
Natale, J., Vitale, S., Isaia, R., 2024. Simultaneous normal and reverse faulting in reactivating caldera faults: A detailed field structural analysis from Campi Flegrei (southern Italy). J. Struct. Geol. 181, 105109. https://doi.org/10.1016/j.jsg.2024.105109.
Orsi, G., 2022. Volcanic and deformation history of the Campi Flegrei volcanic field, Italy. In: Orsi, G., D'Antonio, M., Civetta, L. (Eds.), Campi Flegrei: A Restless Caldera in a Densely Populated Area. Springer, Cham, pp. 1–53. https://doi.org/10.1007/978-3-642-37060-1
Orsi, G., Di Vito, M., Selva, J., Marzocchi, W., 2009. Long-term forecast of eruption style and size at Campi Flegrei caldera (Italy). Earth Planet. Sci. Lett. 287 (1–2), 265–276. https://doi.org/10.1016/j.epsl.2009.08.013.
Palumbo, A., 1985. Influence of external tidal and meteorological forces on the bradyseismic phenomenon in the Phlegraean Fields. IL Nuovo Cimento C 8 (5), 538–551.
Petrillo, Z., Chiodini, G., Mangiacapra, A., Caliro, S., Capuano, P., Russo, G., Cardellini, C., Avino, R., 2013. Defining a 3D physical model for the hydrothermal circulation at Campi Flegrei caldera (Italy). J. Volcanol. Geotherm. Res. 264, 172–182. https://doi.org/10.1016/j.jvolgeores.2013.08.008.
Petrosino, S., Cusano, P., Madonia, P., 2018. Tidal and hydrological periodicities of seismicity reveal new risk scenarios at Phlegraean Area caldera. Sci. Rep. 8, 13808. https://doi.org/10.1038/s41598-018-31760-4.
Ramsay, J.G., 1967. Folding and Fracturing of Rocks. McGraw-Hill, New York, p. 568.
Rolandi, G., Bellucci, F., Heizler, M.T., Belkin, H.E., De Vivo, B., 2003. Tectonic controls on the genesis of ignimbrites from the Campanian Volcanic Zone, Southern Italy. Mineral. Petrol. 79, 3–31. https://doi.org/10.1007/s00710-003-0014-4.
Rolandi, G., Troise, C., Sacchi, M., Di Lascio, M., De Natale, G., 2025. The 1538 eruption at the Campi Flegrei resurgent caldera: Implications for future unrest and eruptive scenarios. Nat. Hazards Earth Syst. Sci. 25, 3421–3453. https://doi.org/10.5194/nhess-25-3421-2025.
Rosi, M., Sbrana, A., 1987. The Phlegrean Fields. Quaderni de "La Ricerca Scientifica", CNR, 175 pp.
Roth, P., Pavoni, N., Deichmann, N., 1992. Seismotectonics of the eastern Swiss Alps and evidence for precipitation-induced variations of seismic activity. Tectonophysics 207 (1–2), 183–197. https://doi.org/10.1016/0040-1951(92)90477-N.
Saar, M.O., Manga, M., 2003. Seismicity induced by seasonal groundwater recharge at Mt. Hood, Oregon. Earth Planet. Sci. Lett. 214 (3–4), 605–618. https://doi.org/10.1016/S0012-821X(03)00418-7.
Scafetta, N., Grigolini, P., Imholt, T., Roberts, J., West, B.J., 2004. Solar turbulence in Earth's global and regional temperature anomalies. Phys. Rev. E 69, 026303. https://doi.org/10.1103/PhysRevE.69.026303.
Scafetta, N., Mazzarella, A., 2021. On the rainfall triggering of Phlegraean Fields volcanic tremors. Water 13 (2), 154. https://doi.org/10.3390/w13020154.
Scuderi, M., Collettini, C., 2016. The role of fluid pressure in induced vs. triggered seismicity: Insights from rock deformation experiments on carbonates. Sci. Rep. 6, 24852. https://doi.org/10.1038/srep24852.
Sibson, R.H., 1996. Structural permeability of fluid-driven fault-fracture meshes. J. Struct. Geol. 18 (8), 1031–1042. https://doi.org/10.1016/0191-8141(96)00032-6.
Sibson, R.H., 2003. Brittle-failure controls on maximum sustainable overpressure in different tectonic regimes. AAPG Bull. 87 (6), 901–908.
Siniscalchi, A., Tripaldi, S., Romano, G., Chiodini, G., Improta, L., Petrillo, Z., D'Auria, L., Caliro, S., Avino, R., 2019. Reservoir structure and hydraulic properties of the Campi Flegrei geothermal system inferred by audiomagnetotelluric, geochemical, and seismicity study. J. Geophys. Res. Solid Earth 124 (5), 5336–5356. https://doi.org/10.1029/2018JB016514.
Tan, X., Tramelli, A., Gammaldi, S., Beroza, G.C., Ellsworth, W.L., Marzocchi, W., 2025. A clearer view of the current phase of unrest at Campi Flegrei Caldera. Science 390 (6768), 70–75. https://doi.org/10.1126/science.adw9038.
Todesco, M., 2021. Caldera's breathing: Poroelastic ground deformation at Campi Flegrei (Italy). Front. Earth Sci. 9, 702665. https://doi.org/10.3389/feart.2021.702665.
Torrente, M.M., Milia, A., 2013. Volcanism and faulting of the Campania margin (Eastern Tyrrhenian Sea, Italy): A three-dimensional visualization of a new volcanic field off Campi Flegrei. Bull. Volcanol. 75, 719. https://doi.org/10.1007/s00445-013-0719-0.
Tramelli, A., Convertito, V., Godano, C., 2024. b value enlightens different rheological behaviour in Campi Flegrei caldera. Commun. Earth Environ. 5, 275. https://doi.org/10.1038/s43247-024-01447-y.
Tramelli, A., Giudicepietro, F., Ricciolino, P., Chiodini, G., 2022. The seismicity of Campi Flegrei in the context of an evolving long-term unrest. Sci. Rep. 12, 2900. https://doi.org/10.1038/s41598-022-06928-8.
Ueda, T., Kato, A., 2019. Seasonal variations in crustal seismicity in San-in District, Southwest Japan. Geophys. Res. Lett. 46 (6), 3172–3179. https://doi.org/10.1029/2018GL081789.
Vanorio, T., Geremia, D., De Landro, G., Guo, T., 2025. The recurrence of geophysical manifestations at the Campi Flegrei caldera. Sci. Adv. 11 (18), eadt2067. https://doi.org/10.1126/sciadv.adt2067.
Wang, C., Manga, M., 2021. Water and Earthquakes. Springer, Cham, 387 pp. https://doi.org/10.1007/978-3-030-64308-9.
Warren, N.W., Latham, G.V., 1970. An experimental study of thermally induced microfracturing and its relation to volcanic seismicity. J. Geophys. Res. 75 (23), 4455–4464. https://doi.org/10.1029/JB075i023p04455.
Wiemer, S., McNutt, S.R., 1997. Variations in the frequency–magnitude distribution with depth in two volcanic areas: Mount St. Helens, Washington, and Mt. Spurr. Alaska. Geophys. Res. Lett. 24, 189–192. https://doi.org/10.1029/96GL03779.
Wyss, M., 1973. Towards a physical understanding of the earthquake frequency distribution. Geophys. J. Int. 31, 341–359. https://doi.org/10.1111/j.1365-246X.1973.tb06506.x.
Zollo, A., Maercklin, N., Vassallo, M., Iacono, D.D., Virieux, J., Gasparini, P., 2008. Seismic reflections reveal a massive melt layer feeding Campi Flegrei caldera. Geophys. Res. Lett. 35, L12306. https://doi.org/10.1029/2008GL034242.